# Geophysical Investigation of the Camp Roberts Sanitary Landfill, San Luis Obispo County, California

W. E. Doll and T. J. Gamey,
Environmental Sciences Division
Oak Ridge National Laboratory
Oak Ridge, Tennessee

and

J. E. Nyquist,
Department of Geology
Temple University
Philadelphia, Pennsylvania

**Submitted to:**
U.S. Army Environmental Center
Environmental Restoration Division
APG-EA, Maryland

**September 7, 2000**

## Table of Contents

## Executive Summary

In May 2000, a suite of geophysical methods was applied at the Camp Roberts Sanitary Landfill, San Luis Obispo County, California. Innovative geophysical instruments and software were integrated with conventional tools for the project. The primary purpose of the investigation was to determine whether the old and new landfills have distinct boundaries, and if they overlap. The project was also designed to characterize the geologic setting of the landfill, and to provide an evaluation of the effectiveness of geophysical tools for subsequent investigations at the site. A small electromagnetic investigation of reported underground storage tanks and/or 55-gallon drums at an armored vehicle maintenance facility was also conducted.

The boundaries of the active and historic portions of the landfill were clearly defined by magnetic mapping. An EM-61electromagnetic survey of a portion of the study area provided results that were as good as those determined by magnetic mapping, but the data were more time-consuming to acquire. Seismic refraction and multielectrode resistivity data provided confirmation of the limits of the landfill areas in profile view.

Tomographic seismic refraction processing software was proven to be superior to conventional delay-time methods for this site because of the heterogeneity of the subsurface and velocity gradients. Depth penetration for the new capacitively-coupled OhmMapper resistivity system was limited because of shallow high conductivities. The Sting multielectrode resistivity system was able to achieve greater penetration, but is more time consuming to use than the OhmMapper system.

None of the methods provided a reliable estimate of the water table. The seismic data were inhibited by heterogeneity and limitations of the delay-time method, but even the vertical seismic profile did not show a velocity transition that corresponded to the measured water table elevation. The resistivity methods were inhibited by a lack of penetration caused by the shallow conducting zone.

Results of this study provide insight into geophysical techniques that could be used to address issues that are relevant to environmental remediation at the site. Magnetic surveys could be used to provide further definition of the boundaries of the landfill. Geophysical methods (seismic refraction combined with time domain electromagnetic (TDEM) or controlled source audio magnetotellurics (CSAMT)) could be integrated with confirmatory drilling to image the water table and bedrock elevation.

# 1 Introduction

During the week of May 1, 2000, magnetic, electromagnetic, electrical, and seismic geophysical data were acquired at the Camp Roberts Sanitary Landfill, San Luis Obispo County, California. The primary purpose of the landfill investigation was to determine whether the old and new landfills have distinct boundaries, and if they overlap. Secondary purposes of the landfill investigation were to determine depth to bedrock beneath the area, to define the lateral extent of the old landfill area, and to evaluate the effectiveness of a suite of geophysical techniques for addressing subsequent site investigations. The acquisition team was composed of staff from Oak Ridge National Laboratory, Temple University, the Los Alamitos Office of the National Guard Bureau, and Lawrence Livermore National Laboratory. In addition, a small electromagnetic data set was acquired at a reported tank site a few miles from the landfill. This report provides a summary of the work that was done, the results of that study, and an interpretation of the data, and some conclusions that may be applicable to subsequent work.

Figure 1 shows a map view of the grid blocks where data were acquired at the Landfill site. In order to define the character of the region between the known portions of the new and old landfills G-858 vertical magnetic gradient data were acquired over Grid Blocks 1-15 in Figure 1. Electromagnetic (EM-61) data were recorded in Area 14 for comparison purposes. Both seismic refraction and multielectrode resistivity data were acquired along the profile lines (red lines in Figure 1) that lie within Grid Blocks 1-15. A vertical seismic velocity profile was acquired in well MW1, about 1500 feet south of the study area. Seismic refraction data (but not multielectrode resistivity data) were acquired along Profile G which crosses this well. The correlation between the velocity profile and the seismic refraction data is used to control interpretation of the other seismic refraction profiles. Multielectrode resistivity data were acquired along Profile F in order to provide a resistivity profile that completely crosses a known trench area. Electromagnetic data were acquired with the Geometrics OhmMapper system in Grid Block 15 and along the A and B profile lines in order to evaluate the effectiveness of this new tool for subsequent investigations at Camp Roberts. Corners for each of the 15 grid blocks and selected points on profile lines were surveyed using a global positioning system (GPS), and elevations along the seven profile lines were determined with a transit.

Magnetic gradiometer data were also acquired south of Grid Blocks 1-15 on nine long traverse lines in order to provide an indication of the southern limit of the old landfill. Six of these nine lines were parallel to one another at 100-200-ft spacing, and the others radiated from a point near the southern extent of the parallel lines. The area surveyed by these nine lines was selected with the assistance of the Los Alamitos Environmental Office staff.

Finally, EM61 electromagnetic data were acquired at a 1-acre site (located about two miles from the landfill) where buried drums and tanks had previously been reported.

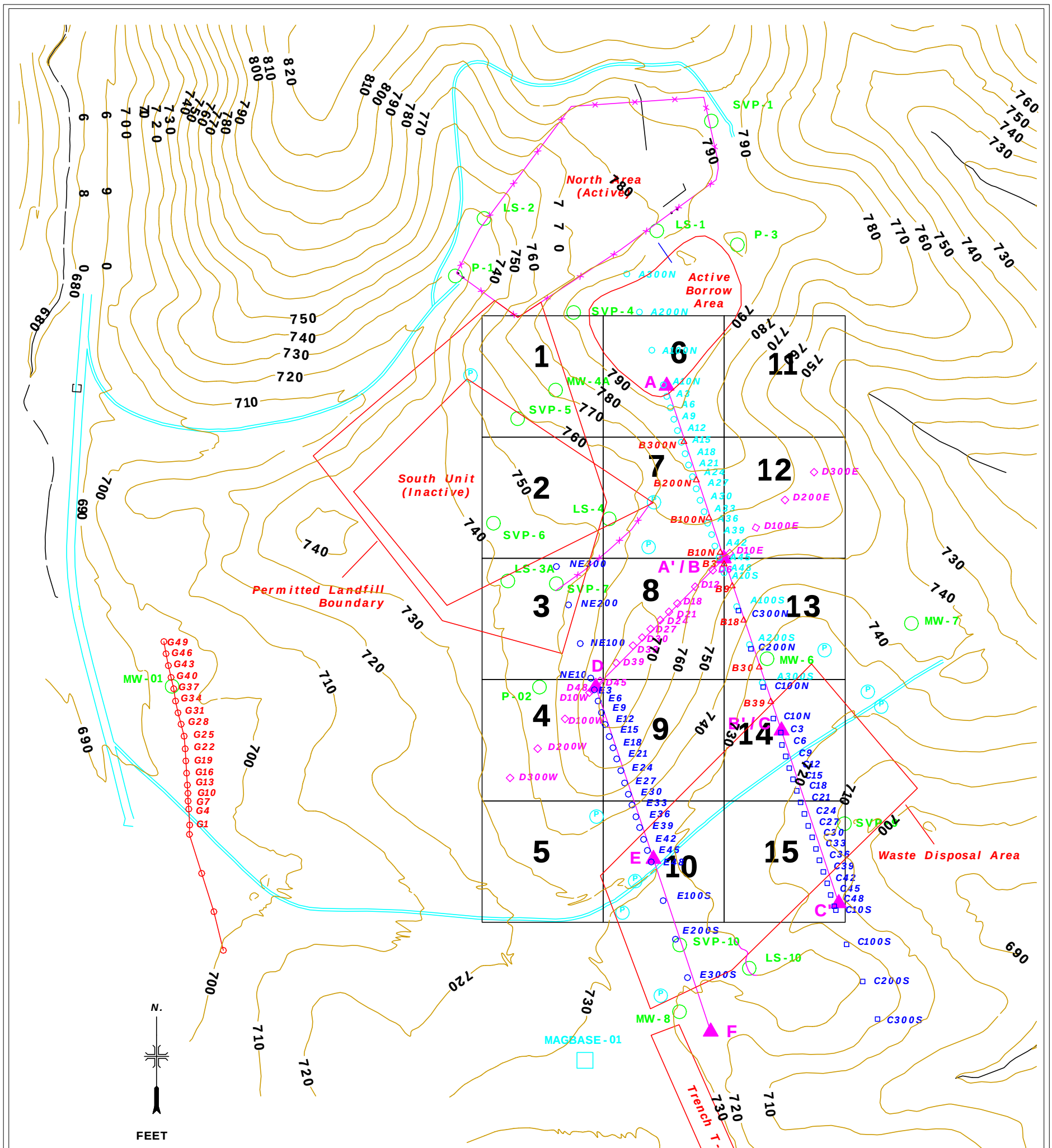


Figure 1: Map of the landfill site showing the 15 areas where magnetic data were acquired, and the locations of Profile Lines A-G.

# 2 Site Description

Camp Roberts, built in 1941-1942, is located about 12 miles north of Paso Robles, California, and consists of high plains, rolling hills, stream valleys totaling more than 42,000 acres. Sparse live oaks are found over much of the facility. The Camp Roberts solid waste disposal facilities are located about two miles south-southeast of the main entrance to Camp Roberts. They include a permitted landfill and at least five waste disposal areas that were closed before the State and County landfill permitting programs came into effect (Geosystems Consultants Inc., 1992). The 14.3-acre permitted landfill consists of an active north unit (Figures 1 and 2) and an inactive south unit (Figure 1).


**Figure 2:** The active landfill area.

The five closed waste disposal areas are all south of the permitted landfill, and consist of a small canyon fill, referred to as the T-1/T-2 disposal area and four trench fills referred to as trenches T-3 through T-6 (Figure 1). This portion of the landfill was developed during peak activities during World War II and the Korean War. Several lysimeter and ground water monitoring wells are located within the landfill area. A photograph taken looking northward across the landfill site is shown in Figure 3.

The surficial geologic map for Camp Roberts (Environmental Science Associates, Inc, 1989) indicates that the rocks exposed at the surface are Cenezoic non-marine sedimentary deposits. Clays and clastic sediments (silts, sands, gravels, and mixed grain-size) are reported in well logs from the top 200 ft (Smith, Gardner, and Dunne, Inc., 1989). Other well logging reports use terminology for lithified rocks that would be derived from each sediment type (e.g. siltstone, sandstone, conglomerate; EMCON Associates, 1990). We infer that the subsurface consists of weathered sedimentary rocks or uncemented alluvial materials. The presence of gravels or conglomerates indicates some degree of stream deposition that would result in a heterogeneous subsurface. The lack of stratigraphic correlation from one well to another provides further evidence of discontinuous alluvial lithologies in the subsurface.

Water table elevations have been measured in several monitoring wells at the site. These elevations range from 570 to 615 ft, where surface elevations range from 700 to 830 ft. A contour map of these data (Geosystem Consultants Inc, 1998, Fig 4) shows a steep northward gradient extending downward from the T-1/T-2 trench area toward the active landfill. The gradient shows the water table dropping more than 40 ft where topography rises 60 ft. Bedrock depths at the site are unknown.

**Figure 3:** Photograph of the closed waste disposal areas.

# 3 DATA ACQUIRED IN THE LANDFILL AREA

## 3.1 Grids and Profile Lines

The grid was established based on surveyed points to form a 1500 by 900-foot grid with 300 by 300-foot subgrids. A total of 15 subgrids were surveyed in all. Latitude and Longitude data were projected into NAD27 UTM US-WUS survey feet to correspond with the extant GIS digital database. Profile lines were 470 ft long with Profiles A, B, and C end-to-end and with the east end of Profile E located at the junction of Profiles A and B. Similarly, Profile E began at the western end of Profile D and was aligned end-to-end with Profile F. The coordinates for the corners of the fifteen grid areas are provided in Table 1. The locations of the ends of the seven seismic/ resistivity profile lines are in Table 2. The locations listed in Tables 1 and 2 are those shown on the map in Figure 1. Table 3 lists the start and end points for the nine magnetic traverse lines that extend south of the magnetic grids, and were intended to delineate the southern extent of the old landfill area.

**Table 1.** Coordinates of Grid Block Corners, in NAD27 UTM US-WUS survey feet.

| Grid Block ID | Southwest Corner | | Northeast Corner | |
|---|---|---|---|---|
| | Easting | Northing | Easting | Northing |
| 1 | 2312380.5 | 12995670.5 | 2312680.6 | 12995970.5 |
| 2 | 2312380.5 | 12995370.4 | 2312680.6 | 12995670.5 |
| 3 | 2312380.5 | 12995070.3 | 2312680.6 | 12995370.4 |
| 4 | 2312380.5 | 12994770.3 | 2312680.6 | 12995070.3 |
| 5 | 2312380.5 | 12994470.2 | 2312680.6 | 12994770.3 |
| 6 | 2312680.6 | 12995670.5 | 2312980.7 | 12995970.6 |
| 7 | 2312680.6 | 12995370.4 | 2312980.7 | 12995670.5 |
| 8 | 2312680.6 | 12995070.3 | 2312980.7 | 12995370.4 |
| 9 | 2312680.6 | 12994770.3 | 2312980.7 | 12995070.3 |
| 10 | 2312680.6 | 12994470.2 | 2312980.7 | 12994770.3 |
| 11 | 2312980.7 | 12995670.5 | 2313280.8 | 12995970.6 |
| 12 | 2312980.7 | 12995370.4 | 2313280.8 | 12995670.5 |
| 13 | 2312980.7 | 12995070.3 | 2313280.8 | 12995370.4 |
| 14 | 2312980.7 | 12994770.3 | 2313280.8 | 12995070.3 |
| 15 | 2312980.7 | 12994470.2 | 2313280.8 | 12994770.3 |

**Table 2.** Coordinates of Ends of Seismic / Multichannel Resistivity Profile Lines, in NAD27 UTM US-WUS survey feet.

| Profile Line ID | North Endpoint | | South Endpoint | |
|---|---|---|---|---|
| | Easting | Northing | Easting | Northing |
| A | 2312838.0 | 12995797.0 | 2312980.0 | 12995370.0 |
| B | 2312980.0 | 12995370.0 | 2313123.0 | 12994944.0 |
| C | 2313123.0 | 12994944.0 | 2313265.0 | 12994517.0 |
| D | 2312980.0 | 12995370.0 | 2312663.4 | 12995052.4 |
| E | 2312663.4 | 12995052.4 | 2312805.4 | 12994626.4 |
| F | 2312805.4 | 12994626.4 | 2312947.4 | 12994199.4 |
| G | 2311591.4 | 12995164.4 | 2311655.3 | 12994710.7 |

**Table 3.** Coordinates of Ends of Nine Magnetic Profile Lines, in NAD27 UTM US-WUS survey feet.

| Line | North Endpoint | | South Endpoint | |
|---|---|---|---|---|
| | Easting | Northing | Easting | Northing |
| 1 | 2312679.7 | 12994470.8 | 2313120.5 | 12992717.0 |
| 2 | 2312873.4 | 12994525.0 | 2313347.0 | 12992623.5 |
| 3 | 2313047.4 | 12994642.0 | 2313516.7 | 12992765.3 |
| 4 | 2313222.0 | 12994775.9 | 2313715.2 | 12992797.4 |
| 5 | 2313407.1 | 12994849.4 | 2313915.5 | 12992830.9 |
| 6 | 2313391.2 | 12993261.7 | 2313920.6 | 12992822.1 |
| 7 | 2312660.9 | 12993350.7 | 2313390.8 | 12993267.5 |
| 8 | 2313372.7 | 12993271.1 | 2312702.0 | 12993152.4 |
| 9 | 2312933.8 | 12994703.0 | 2313394.5 | 12992838.7 |

## 3.2 Magnetic Survey of the Landfill Area

By making precise measurements of the earth's magnetic field and subtracting the expected magnetic field of the earth from these measurements, one can map magnetic values that differ from the expected (earth dipole) values. These values are referred to as magnetic anomalies. They are caused by some combination of man-made ferrous metallic objects and naturally occurring magnetic soils and rocks. Magnetic mapping provides an effective tool for determining the spatial distribution of buried metals, particularly where there are few magnetic minerals in the host soil and/or rock. The strength and shape of magnetic anomalies depends on many factors, including the size, shape, and composition of the source, the distance between the source and the magnetometer, and the effects of the host rock and soil cover. Thus it is difficult to determine the precise character of the magnetic anomaly source without additional information. In landfill investigations, the location of buried wastes is usually more important than determining the size and precise locations of individual objects, so magnetic surveys are commonly used.

The Geometrics G-858 magnetic gradiometer, equipped with an AG-132 GPS positioning system with Omnistar differential correction was used for this survey (Figure 4). The G-858 was operated in vertical magnetic gradient mode by simultaneously recording with one magnetometer positioned approximately 1.6 ft directly above the other. The bottom magnetometer was kept at approximately 1.3 ft off the ground during data acquisition. The magnetic field was recorded in the instrument memory ten times per second at both magnetometers, and position was recorded every second, resulting in measurements at spatial intervals of approximately 1.2 ft along profile lines. The precise spacing of measurement points was determined by the walking speed of the operator, which was in turn related to topography and walking direction. The AG-132 has an indicator that assists the operator in maintaining the proper direction for each line. In addition, orange highway cones were used to provide a visual target at the ends of the lines. Care was taken to keep vehicles and other crew members away from the magnetometer during data acquisition to eliminate possible sources of noise.

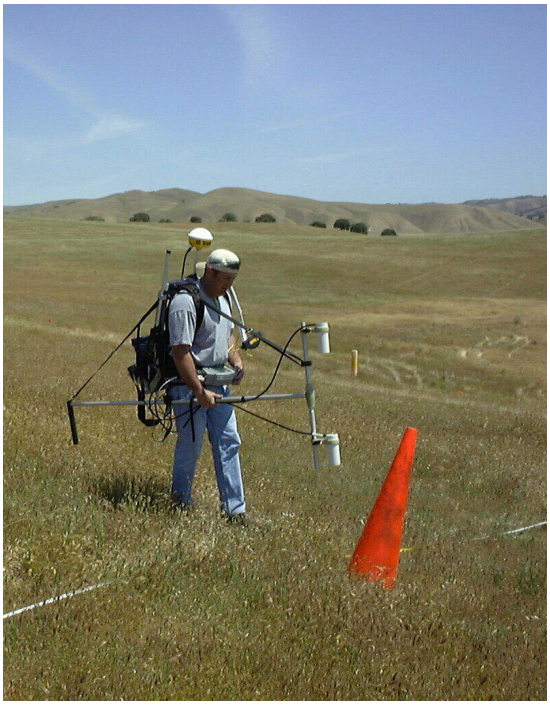

**Figure 4:** Geometrics G-858 magnetic gradiometer with GPS positioning.

Data processing steps included downloading from the data logger to a computer, registration of lines, conversion to Geosoft data format, integration of data from the 15 areas into a single file, editing, gridding, and contouring. No filtering of the data was required, although several data dropouts were removed. The field QC process determined that the data quality on several lines was inadequate and they were re-surveyed at the time. Two partial lines were later determined to have faulty GPS positioning and were removed, causing a small gap in the final coverage. Numerous map products may be produced from the data. Both total field and vertical gradient data are measured directly. For the purposes of this project, the total magnetic gradient (or analytic signal) is presented due to its intuitive interpretation properties for landfill sources. The total magnetic gradient map for the landfill area is shown in Figure 5. Plate 1 shows these data with previously mapped landfill boundaries and well locations overlain. Figure 6 shows a 3-D display of topography with total magnetic gradient overlain as color-coded contours.

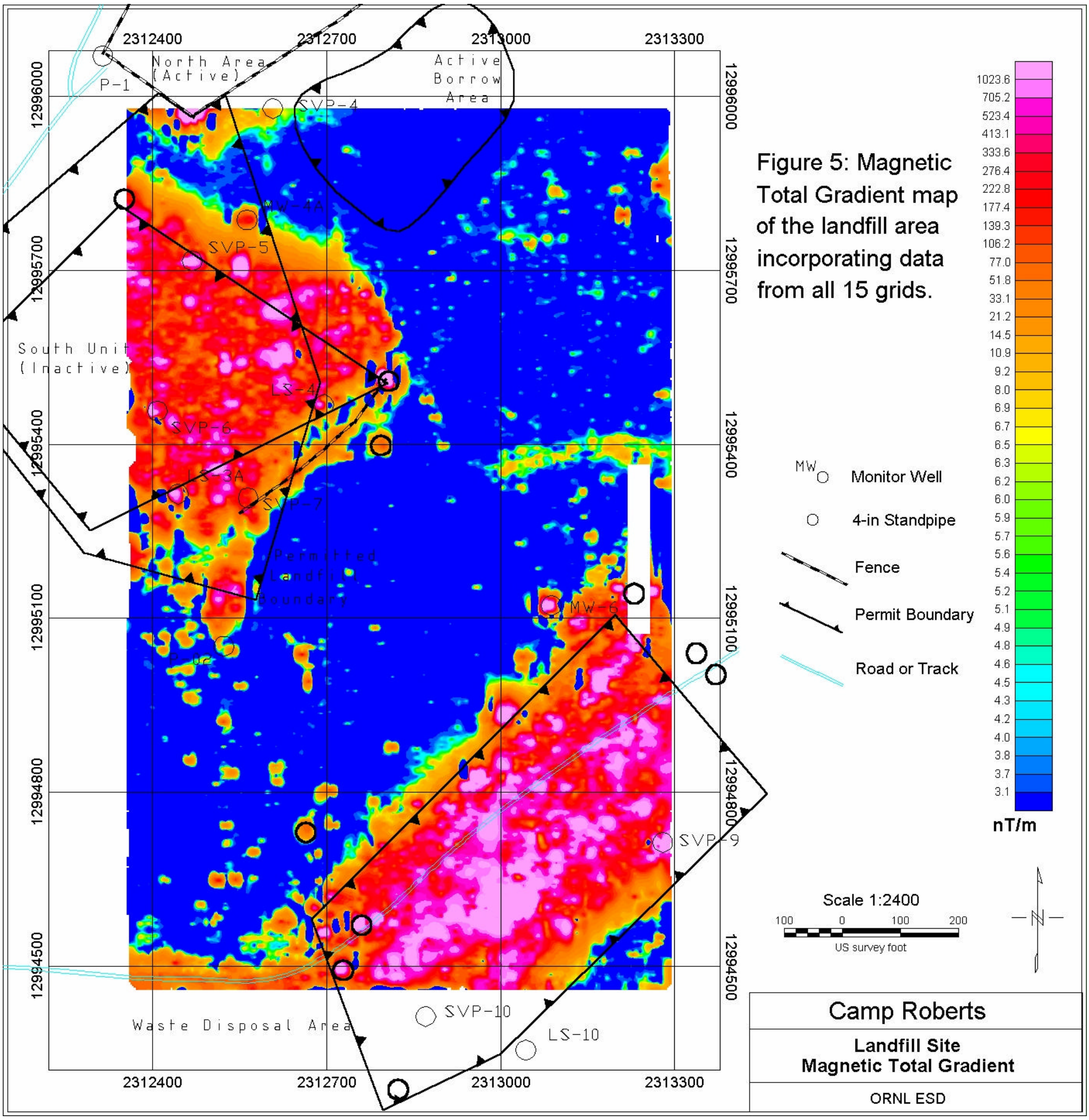
2312400
2312700
2313000
2313300
12996000
12995700
12995400
12995100
12994800
12994500
North Area (Active)
Active Borrow Area
South Unit (Inactive)
Waste Disposal Area
Permitted Landfill Boundary
P-1
SVP-4
MW-4A
SVP-5
LS-4
SVP-6
LS-3A
SVP-7
MW-6
SVP-9
SVP-10
LS-10
Figure 5: Magnetic Total Gradient map of the landfill area incorporating data from all 15 grids.
1023.6
705.2
523.4
413.1
333.6
276.4
222.8
177.4
139.3
106.2
77.0
51.8
33.1
21.2
14.5
10.9
9.2
8.0
6.9
6.7
6.5
6.3
6.2
6.0
5.9
5.7
5.6
5.4
5.2
5.1
4.9
4.8
4.6
4.5
4.3
4.2
4.0
3.8
3.7
3.1
nT/m
MW Monitor Well
4-in Standpipe
Fence
Permit Boundary
Road or Track
Scale 1:2400
100 0 100 200
US survey foot
Camp Roberts
Landfill Site
Magnetic Total Gradient
ORNL ESD

## 3.3 Magnetic Traverses to Assess the Southern Boundary of the Old Landfill

In addition to the magnetic data acquired in the fifteen grid sectors, the G-858 system was used to acquire magnetic data along nine traverse lines that extend from the southern portion of the grid. The purpose was to provide evidence to support or refute earlier determinations about the southern extent of the old landfill. The AG-132 positioning system was used to maintain the line orientation, and position was recorded on the G-858 data logger as before. The data that were acquired during these traverses are displayed in Figure 7 along with the southern portion of the grid where they overlapped.

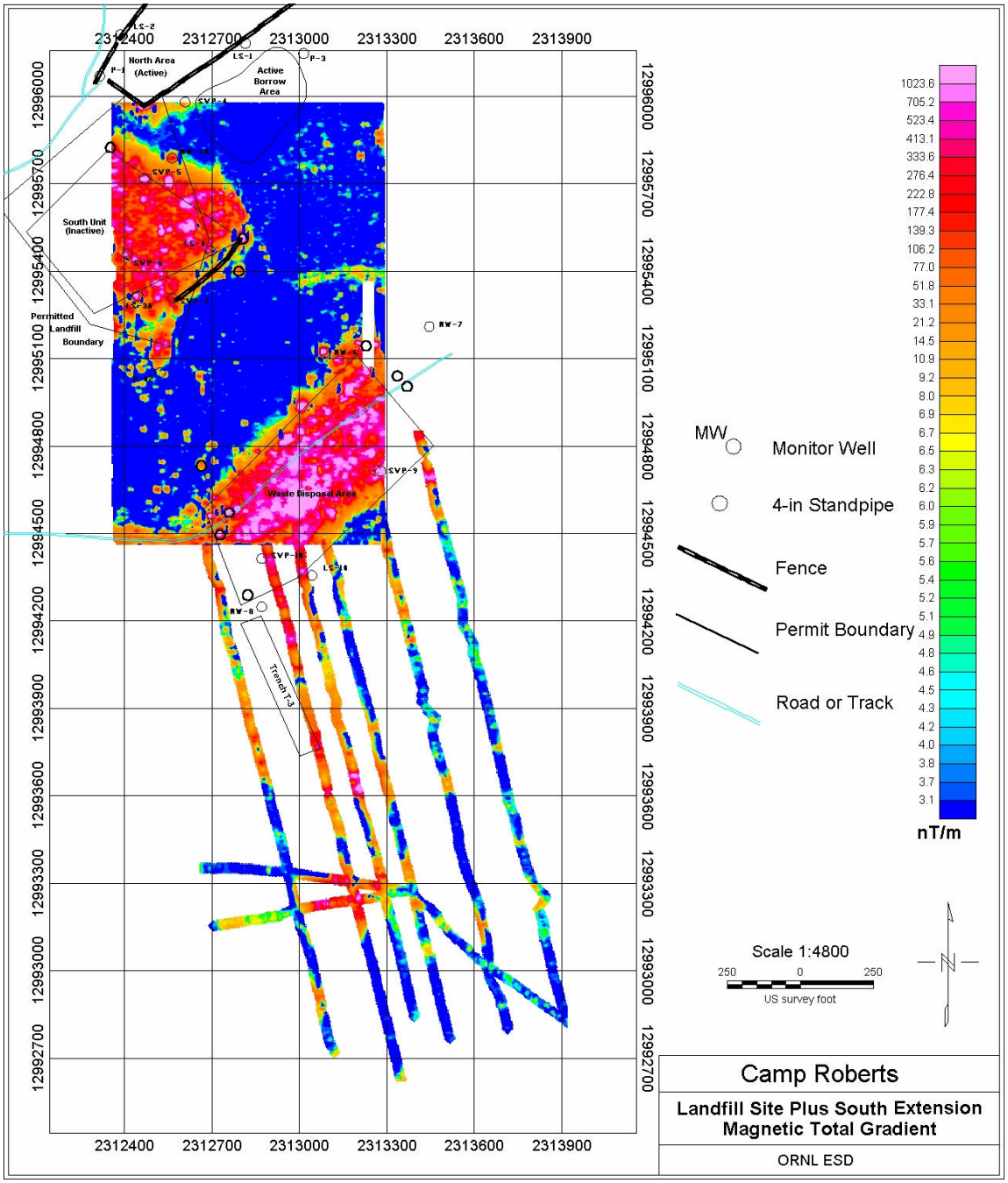

## 3.4 EM-61 Survey of Section 14 of the Landfill Grid

Electromagnetic (EM) methods use a transmitter to broadcast a radio-frequency signal into the ground. This signal induces small electric currents to flow in the soil, rock, and any buried objects near the transmitter. The more conductive the targets are, the larger the electric current that is induced and the longer it persists. Receiver coils measure the signal produced by these induced currents. EM methods provide a rapid, inexpensive means of surveying large areas and are able to detect non-ferrous metals that might not be detected by a magnetometer.

**Figure 8:** Geonics EM-61 electromagnetic system.

The Geonics EM61 metal detector consists of two square coils measuring 1m X 1m mounted on a pair of bicycle wheels and towed behind the operator (Figure 8). The operator wears a backpack unit that contains the control unit and data logger. One coil serves as both transmitter and receiver, while the second is only a receiver, located about one foot above the first. The EM61 is a time-domain instrument that transmits a short pulse from the transmitting coil, and then records the amplitude of the response in both coils at a selected time after the pulse is shut off. The response is recorded after the currents from the more resistive earth have decayed so that the instrument responds primarily to buried metal. The EM61 should be able to detect large metal objects to depths of 7m or more.

As a means of comparing the effectiveness of magnetic and electromagnetic methods at the site, EM61 data were acquired in Area 14 of the landfill. Positioning was controlled with flags and tape measures, as a GPS tracking system was not available for this instrument. Figure 9 shows a comparison between the EM61 data and the G858 data from Area 14.

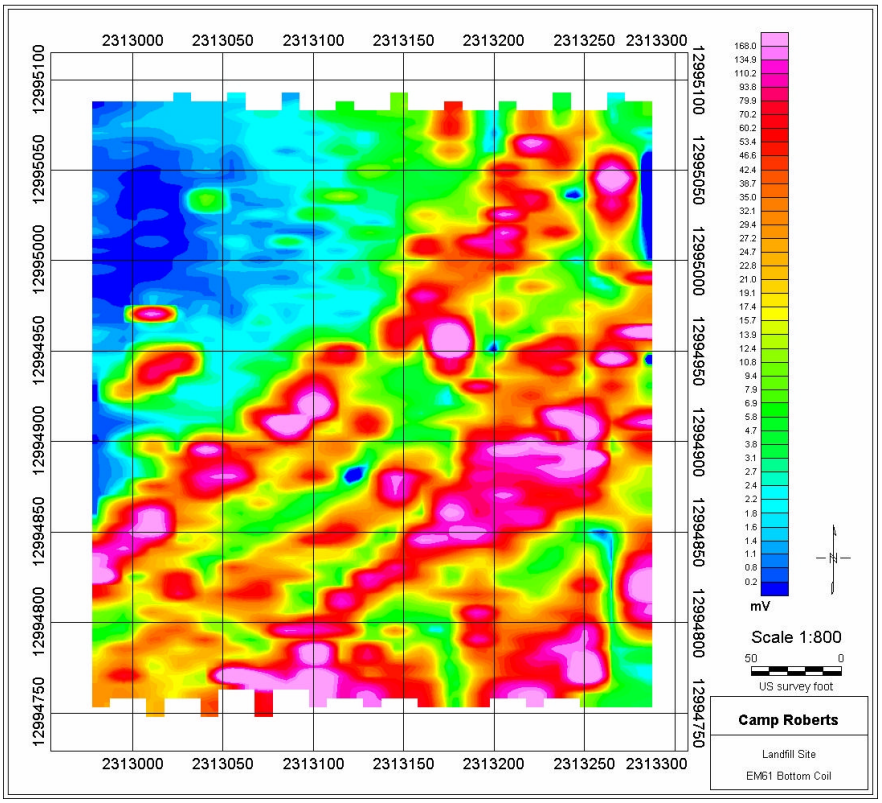


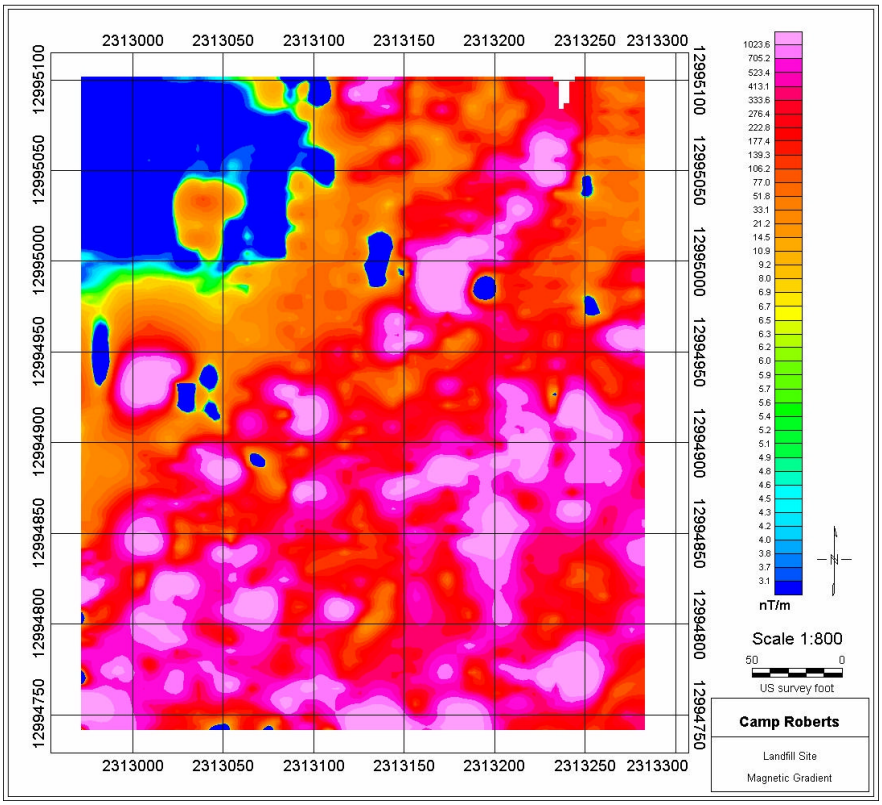


**Figure 9:** A comparison of EM61 data (top) and magnetic gradient (bottom) data over subgrid 14.

## 3.5 Seismic Refraction Surveys of the Landfill Area

The seismic refraction method is commonly used to determine depth to bedrock, the water table, or some other geologic interface that separates media through which seismic waves propagate at different velocities. The interfaces need not be planar, and typically do not have a large dip, and the velocities of the layers are assumed to increase with depth. Conventional data analysis methods assume that layers are laterally continuous and that the velocities that are assigned to each layer are constant within that layer. These assumptions can be proven by inspection of the data and by comparison of seismic refraction data with surface to borehole measurements known as vertical seismic profiles.

In layered media, the first seismic energy to reach a receiver from a selected shot location will sometimes travel through a deeper high velocity layer, just as drivers can often reach their destination sooner by traveling in the 'fast lane'. Time that may be lost in traveling through slow surface layers is recovered by the time saved by traveling at higher velocity. Seismic refraction methods provide an image of subsurface layering by measuring the time of the first arriving wave for each receiver given known shot point and receiver locations. Time vs. receiver distance plots can be used to calculate structural cross sections that would yield such first arrival times. By combining results for several shotpoints into the stationary receiver array, a robust solution can be obtained that includes dips and structural variations on each interface in the model, as long as the a priori assumptions are correct. More recently, tomographic inversion routines are being marketed for processing of seismic refraction data. These routines require more shot points within the receiving array, but allow laterally discontinuous layers, vertical velocity gradients, and lateral changes in velocity. Both conventional processing methods and the newer tomographic methods can be used to detect man-made disturbed zones such as landfills or trenches. In conventional methods, these might be seen as localized thickening or thinning of shallow layers, or as variations and localized changes (increase or decrease) in the slope of the time-distance plot. Tomographic methods could assign higher or lower velocities to such zones, depending on how the velocity was affected by the disturbance.

**Figure 10:** The elastic wave generator (EWG) seismic energy source.

Seismic refraction data were acquired on 6 profile lines, shown as A,B,C,D,E, and G on Figure 1. The data were acquired with a Bison Elastic Wave Generator II (EWG) source (Figure 10), 48 Input/Output Model SM-24/UB 10 Hz geophones, and recorded with a Geometrics Strataview portable seismograph. The geophones were spaced at 10-ft intervals. Data were acquired at source (shot) intervals of 30-ft within the geophone spread, and at offsets of 10, 100, 200, and 300 ft from each end of the spreads.

**Figure 11:** Equipment used for vertical seismic profile at well MW-1.

Selected shots were used to build velocity profiles for each line using the SIP family of routines (Rimrock Geophysics, 1995). The SIPT-2 code allows co-processing of up to 7 shots for each geophone spread. First arrivals were picked using the SIPIK code. Picking was difficult with the Roberts data because the first arrivals have very low frequency content, and thus are "emergent" (the amplitude builds slowly, rather than abruptly). These attributes of the first breaks result in a higher likelihood of having a few milliseconds of error in the selected arrival times, and can result in a final model that is less precise. Once first breaks were selected, they were incorporated into a data file for each profile line, using the SIPIN and SIPEDT codes. The data file includes precise positions for each geophone and shot point, and all of the first arrival picks. Each pick was assigned to a specific subsurface layer in the data file. For the Camp Roberts data sets, this was more difficult than for some sites because the data indicate that velocities increase gradationally, rather than abruptly, with depth. SIPT-2 processing assumes that there are discrete layers that are laterally continuous and have constant velocity. Thus the layers that we selected in processing these data are an approximation that assumes constant velocity layers.

Vertical seismic profile data were acquired in well MW-1, which is located near Geophone 38 of Line G. The EWG was used as a source, and data were recorded with a Geostuff Model BHG-2C downhole geophone at 5-ft intervals in the well, extending from 5-ft depth to 140-ft depth, with the source offset at 7 ft. The data that were acquired in this well are shown in Figure 12, and a plot of the calculated velocities is shown in Figure 13. The interval velocities that were calculated are shown as filled circles. These were smoothed with a three-point average to yield the values shown by the X's that are connected by a fine line. The bold continuous line shows the velocity profile that was calculated at Geophone 38 from the Line G seismic refraction data.

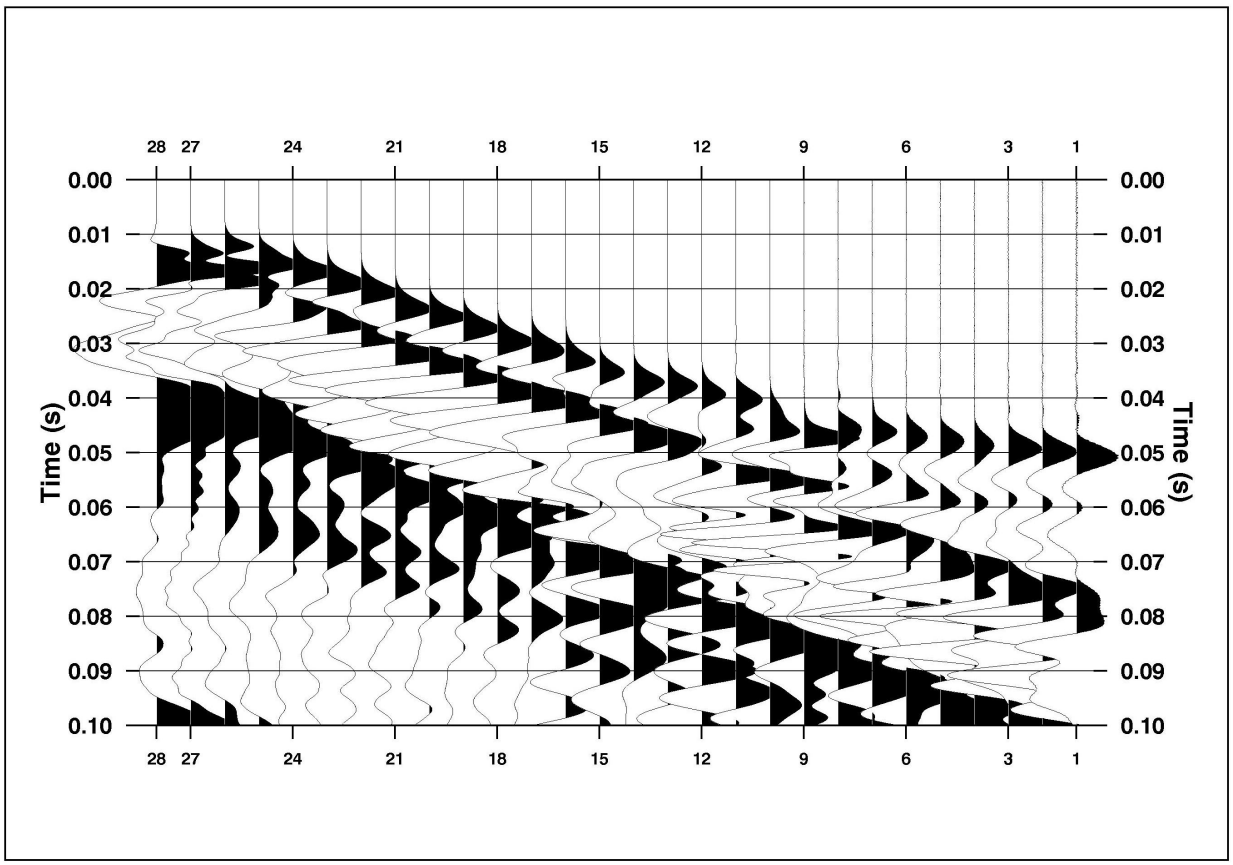


**Figure 12:** Vertical seismic profile data for well MW-1. Data were acquired at 5-foot intervals beginning at 140 ft (trace number 1, right hand side) up to 5 ft (trace number 28, left hand side) at an offset of 7 ft from the well casing.

The cross-sections that were determined for Lines A-E and G, based on analysis with the SIP software are shown in Figures 13 through 16. A comparison of velocities derived from the vertical seismic profile (Figure 12) and the seismic refraction profile (Figure 16) is shown in Figure 17. The data from Lines B and C were analyzed with the RAYFRACT software package as a courtesy by Intelligent Resources Inc, the vendor of the software. The RAYFRACT code is one of several new tomographic inversion codes for seismic refraction data. The results of their analysis are shown in Figure 18.

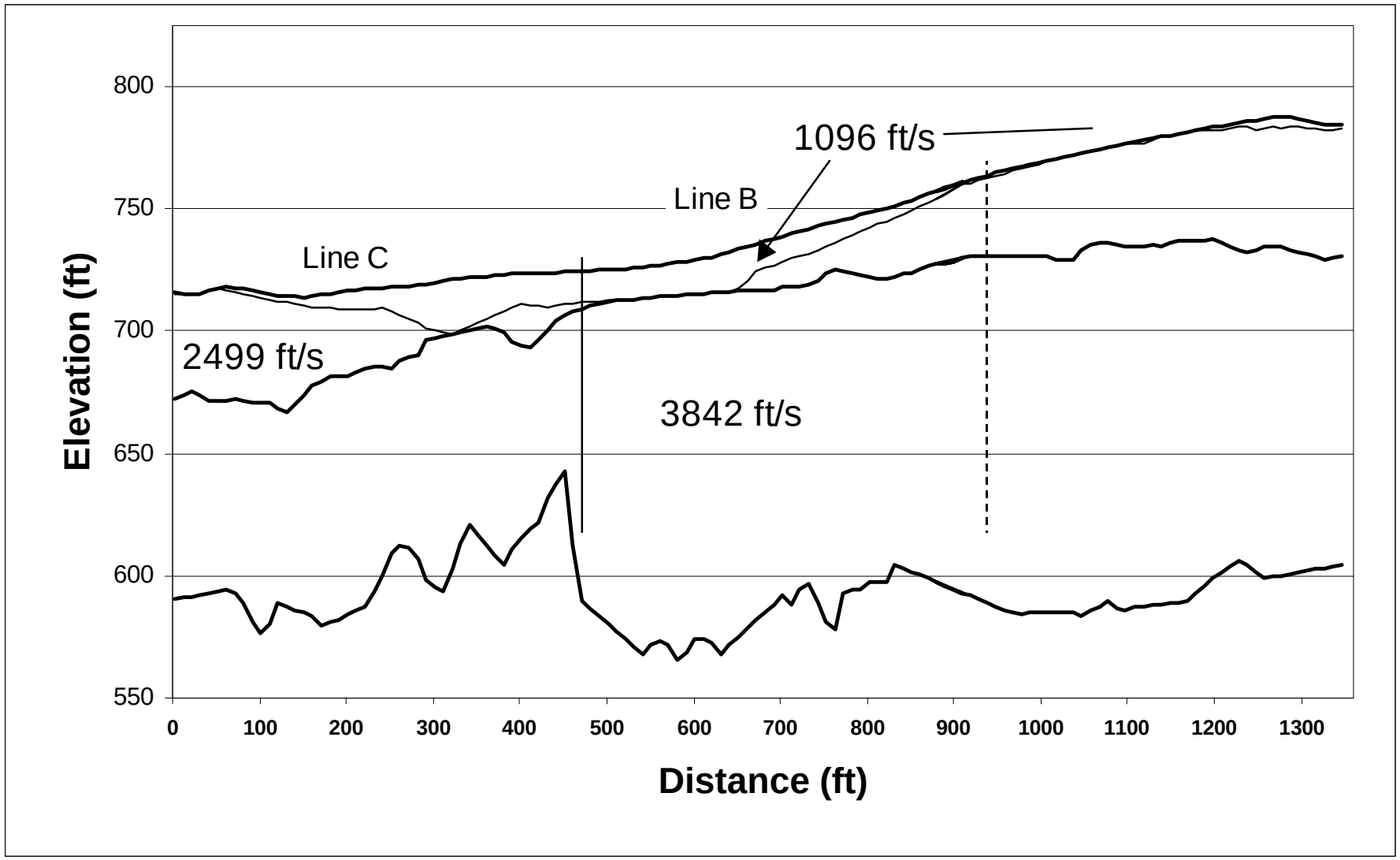


**Figure 13:** Seismic refraction model determined for Lines A, B, and C. Vertical scale is exaggerated.

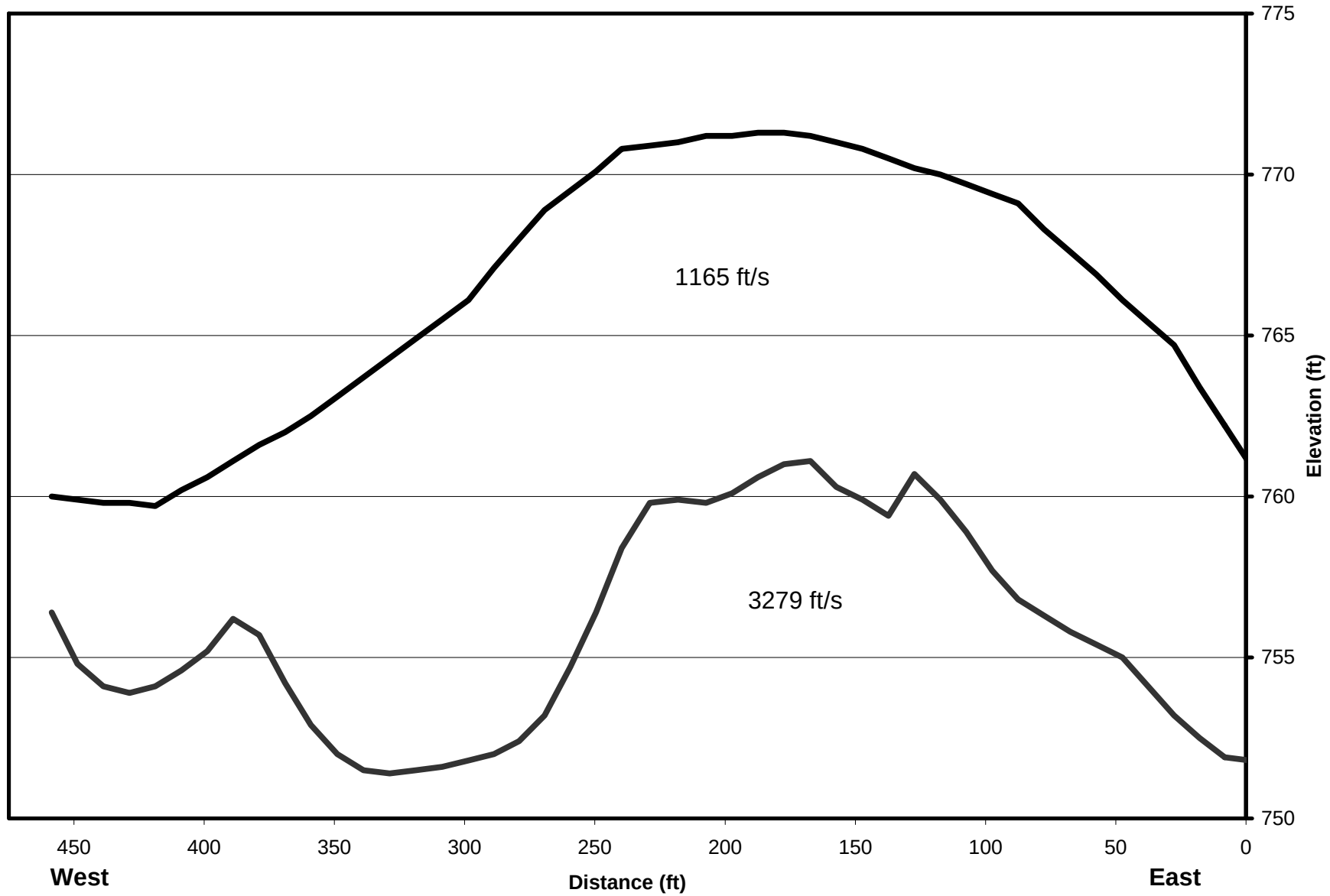


**Figure 14:** Seismic refraction model determined for Line D.

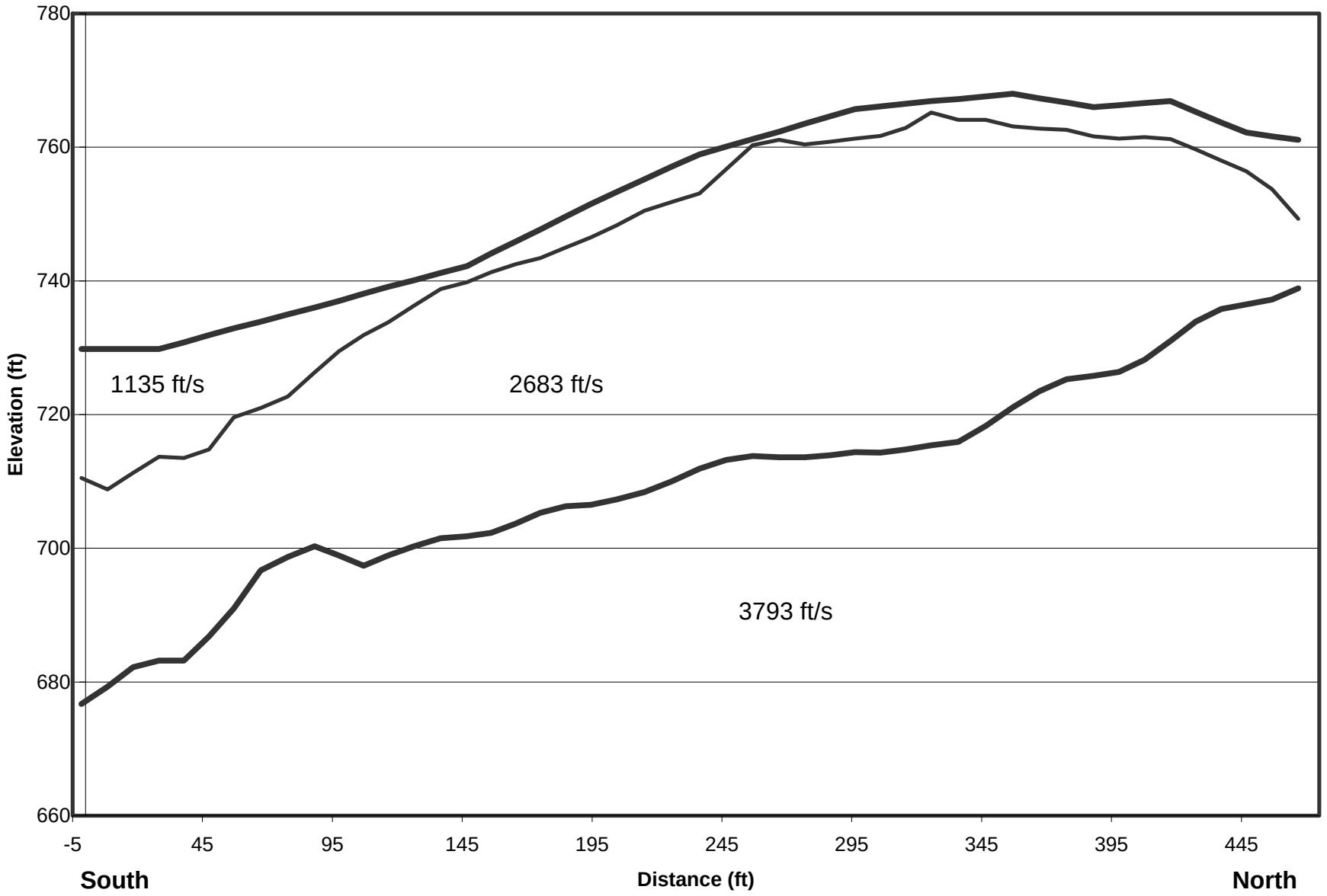


**Figure 15:** Seismic refraction model determined for Line E.

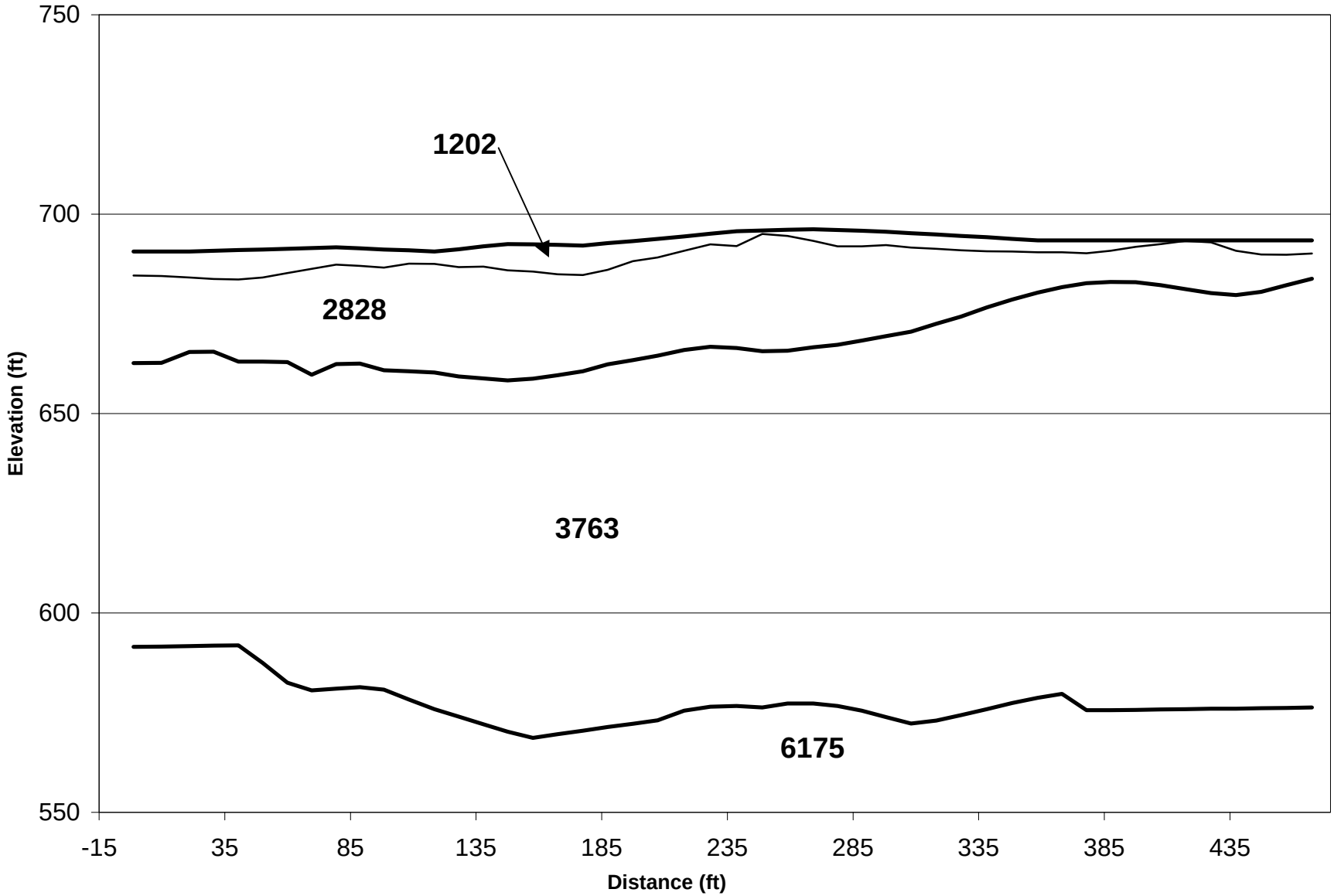


**Figure 16:** Seismic refraction results for Traverse G.

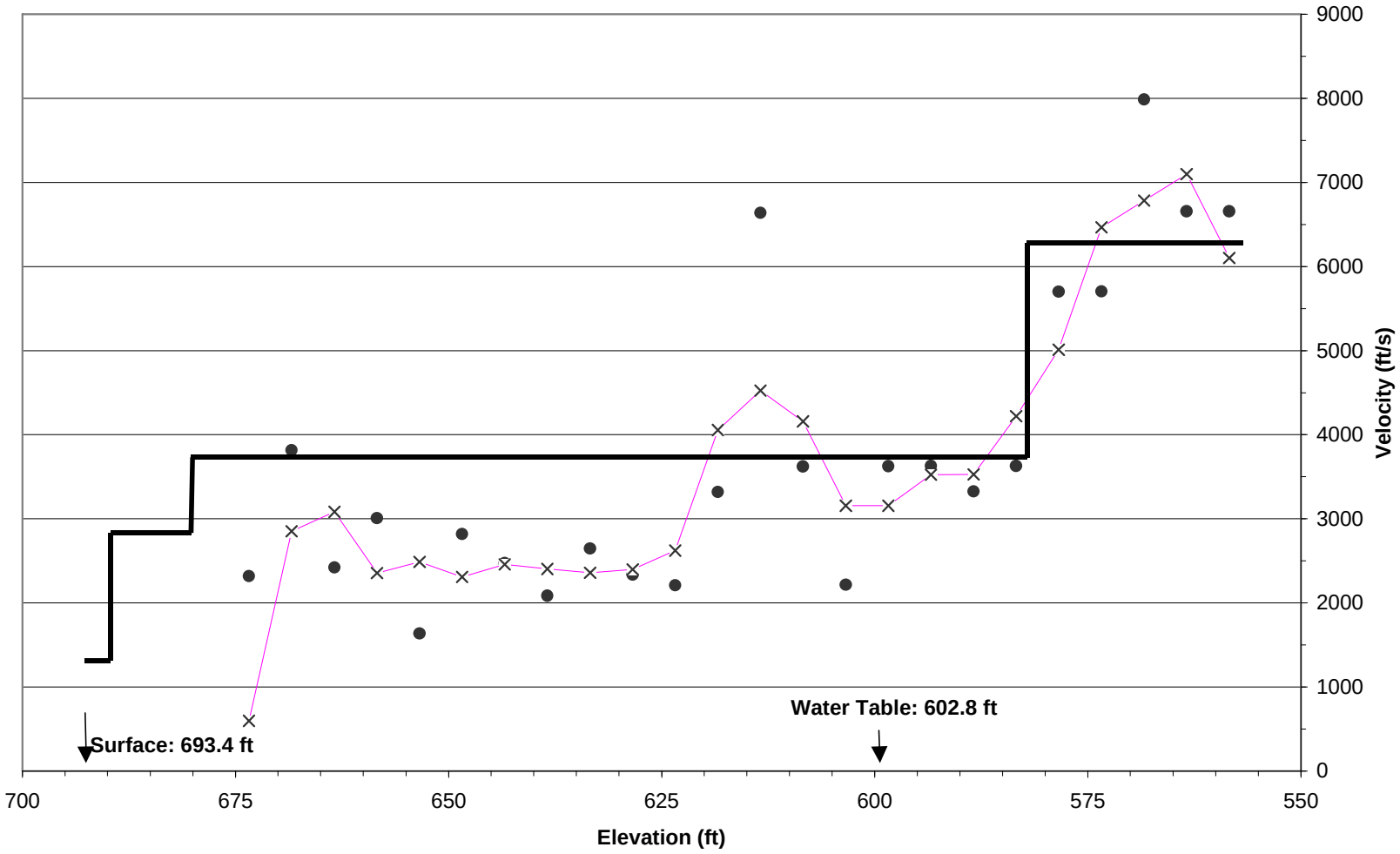


**Figure 17:** Vertical seismic profile for well MW-1, compared with the seismic refraction model for Line G. The velocities derived from the VSP data are represented by round black dots, and a three-point average of these points are shown as the x's that are aconnected by the pink line. The solid black line represents the velocity structure at the well that was modeled from the seismic refraction data. The measured depth of the water table is also shown.

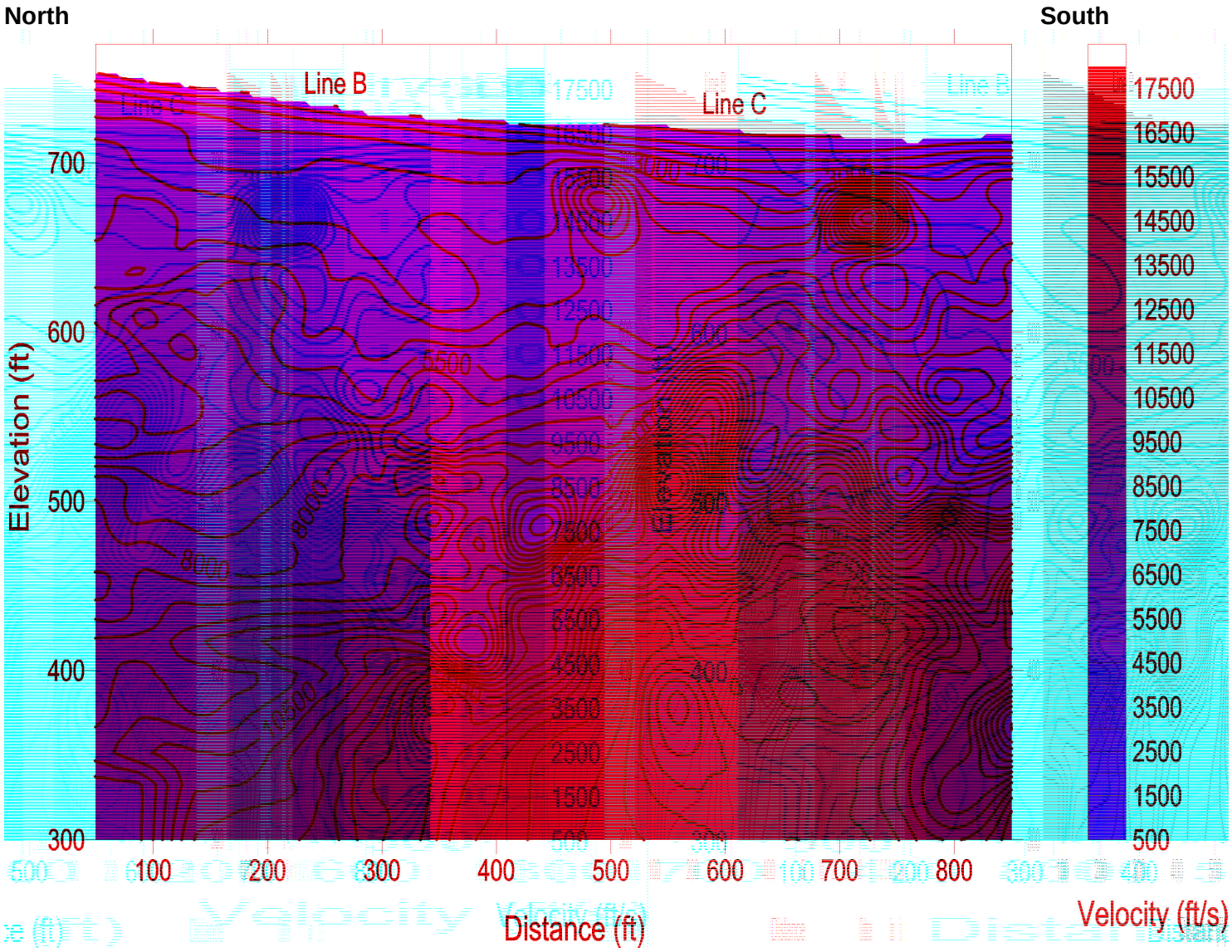


**Figure 18:** Tomographic inversion of Lines B and C determined from RAYFRACT processing

## 3.6 Multielectrode Resistivity Profiling

The principle behind direct current (DC) resistivity measurements is simple. Metal stakes are driven into the ground and a connected to a battery. Geologic structure and manmade buried objects influence the resulting underground flow of electrical current, and this can be measured by mapping the distribution of voltages at the surface.

Most rocks and soils are insulators. The flow of electrical current in the ground is predominantly by electrolytic conduction – ions migrating through water in the pore spaces. Consequently, the electrical resistivity of geologic materials is controlled largely by amount of porosity, the degree of saturation, and the ionic strength of the pore waters. A tight rock will be more resistive than a porous one; a dry rock will be more resistive than a wet one; a rock that does not contribute ions to the pore fluid will be more resistive than one that does. Man-made objects, particularly those containing metals, also reduce the electrical resistivity of the subsurface. The goal of resistivity surveys is to deduce information about rock and soil types, porosity, saturation, and the distribution of man-made objects by their affect on electrical current flow in the ground.

Multielectrode resistivity data were acquired at the Camp Roberts landfill area along survey lines designated A-F(Figure 1) and a single deeper sounding that included line E and F. Data were collected using a 28-electrode Sting/Swift resistivity system (Figure 19) and inverted with the program Res2Dinv. For lines A-F, we used an electrode spacing of 19.7 ft, and for the deeper sounded we used an electrode spacing of 39.4 ft. A dipole-dipole sounded was performed on all of the lines, and with Schlumberger soundings performed on lines C-F and on the deeper sounding.

The setup procedure consisted of flagging the electrode locations using a measuring tape, hammering the stainless steel electrodes roughly 1 ft deep into the ground, and pouring about a liter of salt-saturated water on the stakes to ensure good electrical contact with the ground. The electrode cable was then laid out and the electrodes attached to the metal stakes with rubber bands.

The microprocessor in the Swift resistivity box controlled the firing sequence of the electrodes according to the type of array selected, and logged all of the data, which were downloaded to a laptop computer in the field at the end of each sounding. Each line took roughly 30-45 minutes to setup, an hour to collect data for each array type measured, and 30 minutes to take down, for a total time of about 2 hours per line (3 hrs for lines where we made both dipole-dipole and Schlumberger soundings).

**Figure 19:** Sting/Swift multielectrode resistivity system in the field at Camp Roberts.

### 3.6.1 Results for Sting/Swift Lines A-C

Line A was over undisturbed ground. Line B straddled the boundary between the undisturbed area and the waste area as delineated by the magnetic data. Line C is almost entirely within the waste area. Figure 20 shows a portion of the analytic signal magnetic data with the locations of part of line B and all of line C superimposed. The extent of the burial area is clear and the boundary is quite sharp. With the exception of monitoring wells and occasional scrap metal, there were almost no magnetic anomalies along resistivity line B, whereas line C is clearly over the burial ground.

Lines A-C are collinear, and combine to form a single transect that ran roughly N-S from the top of the hill down to the bottom, across the road, and across the southern disposal area (Figures 21-23).

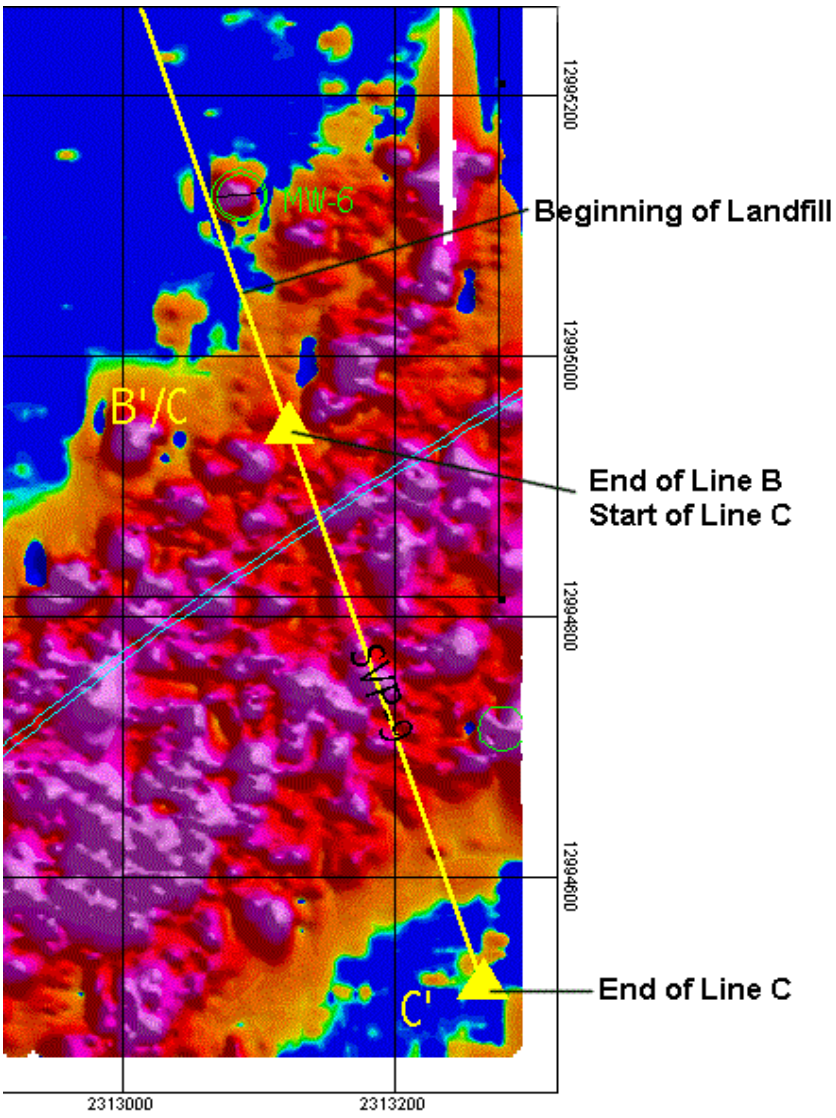


**Figure 20:** Extract of the Magnetic Analytic Signal showing where Line B crosses into the southern disposal area. Coordinates are UTM (ft)

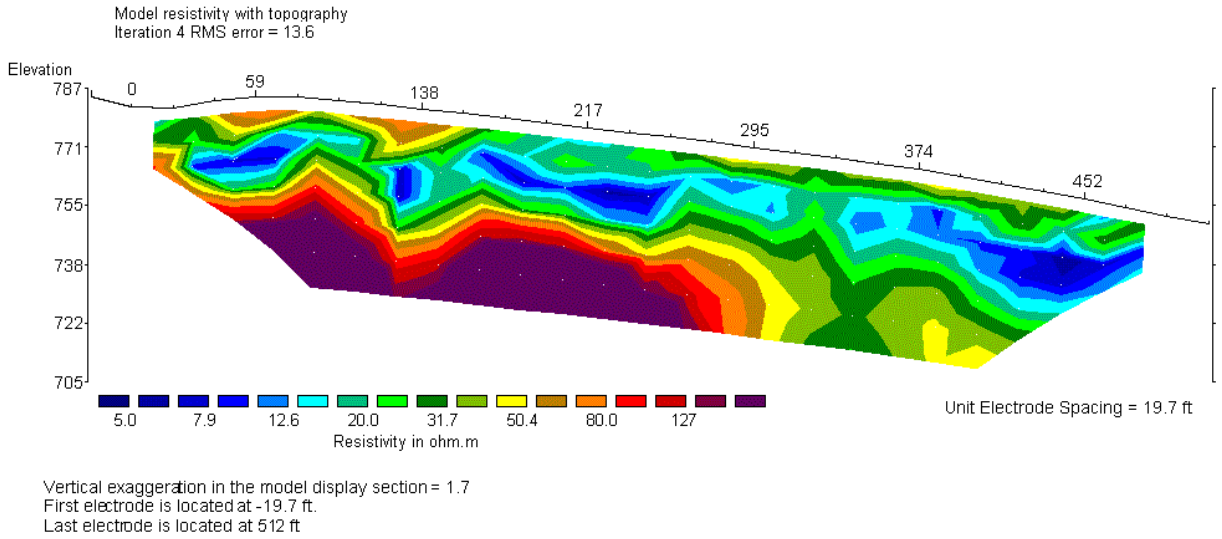


**Figure 21:** Resistivity cross section for Line A. The vertical scale is elevation above mean sea level (m). The horizontal scale is distance along the line (m). The line runs north (left) to south (right).

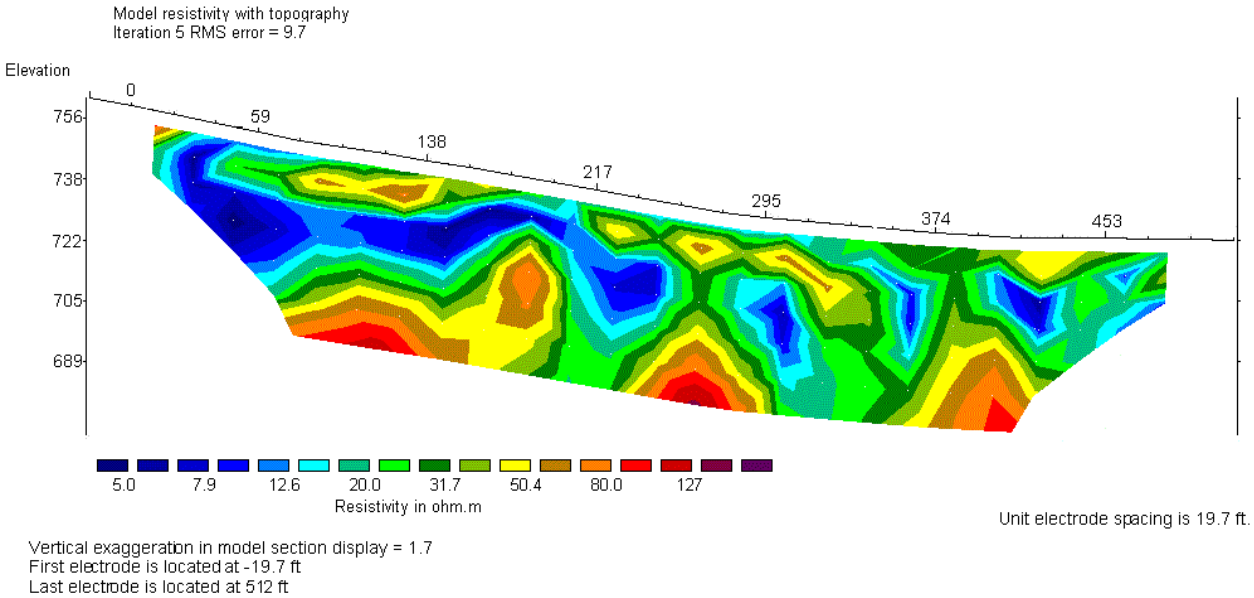


**Figure 22:** Resistivity cross section for Line B. The disruption of the layering at the southern end (right side) of this line is probably due to the excavation and fill associated with the southern landfill.

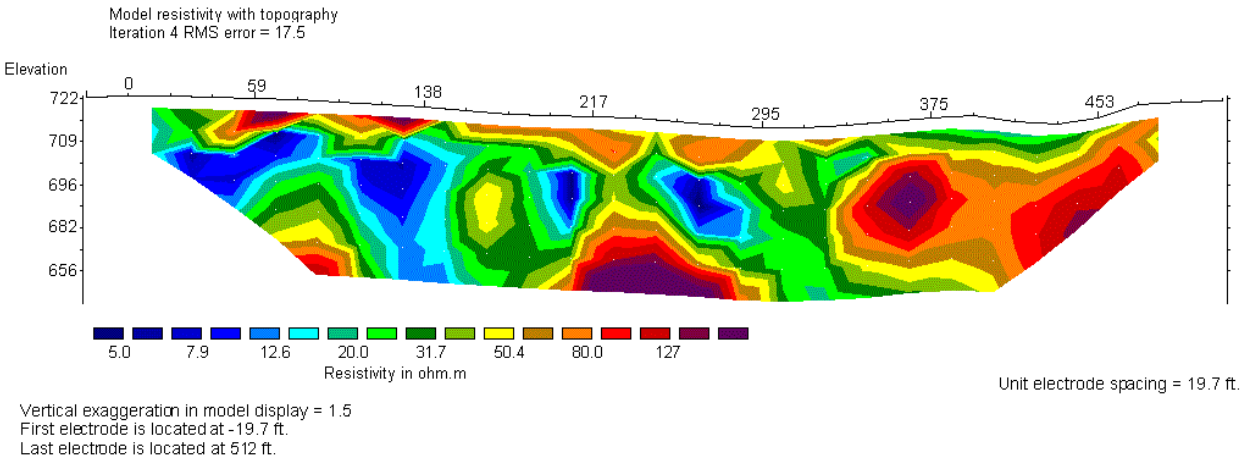


**Figure 23:** Resistivity cross section for Line C. This line is within the southern burial ground and show disrupted layering.

### 3.6.2 Sting/Swift Results for Line D

Line D ran approximately E-W, linking the two N-S transects. It was located entirely outside of both the old and new burial grounds. The line was run parallel to the topographic contours, so it is nearly flat (Figure 24).

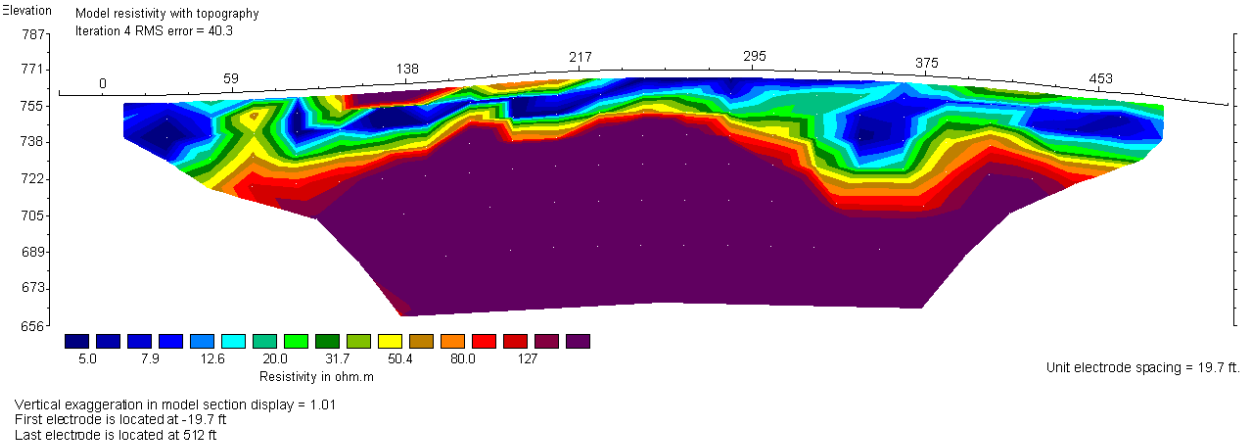


**Figure 24:** Line D shows the same extremely conductive (low resistivity) near-surface layer as Line A.

A dipole-dipole array is the preferred choice when mapping shallow heterogeneity, such as buried metal objects, but because the potential electrodes are positioned outside of the current electrodes (Figure 25), and the current electrodes are close together, there is little current flowing near the potential electrodes, so the voltages are small, making this type of array vulnerable to noise. The conductive near-surface layer makes this problem worse. Conversely, the Schlumberger array (Figure 25) places the potential electrodes between the current electrodes, where more current is flowing, so the array is less sensitive to noise, but the price is lower sensitivity to shallow buried objects. Figure 26 shows the result of a survey along Line D with a Schlumberger array. Figure 27 uses a different color scale for the dipole-dipole data in Figure 24 to facilitate comparison of the deep response for the two array types.

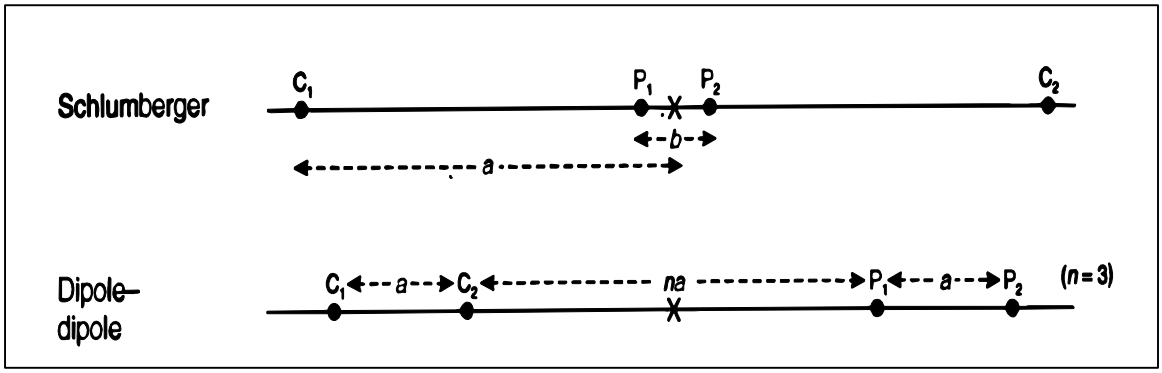


**Figure 25:** Two resistivity array types used at Camp Roberts. C1 and C2 are the current electrodes; P1 and are the potential electrodes. The dipole-dipole array is better for detecting shallow buried objects, but is more sensitive to noise and does not probe as deep as the Schlumberger array.

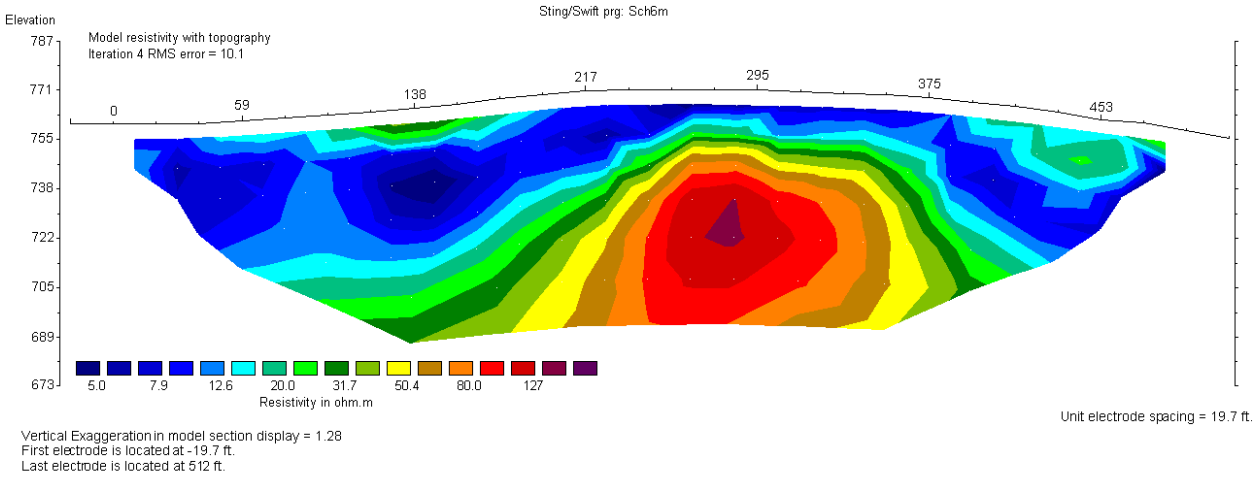


**Figure 26:** Results for Line D using a Schlumberger array.

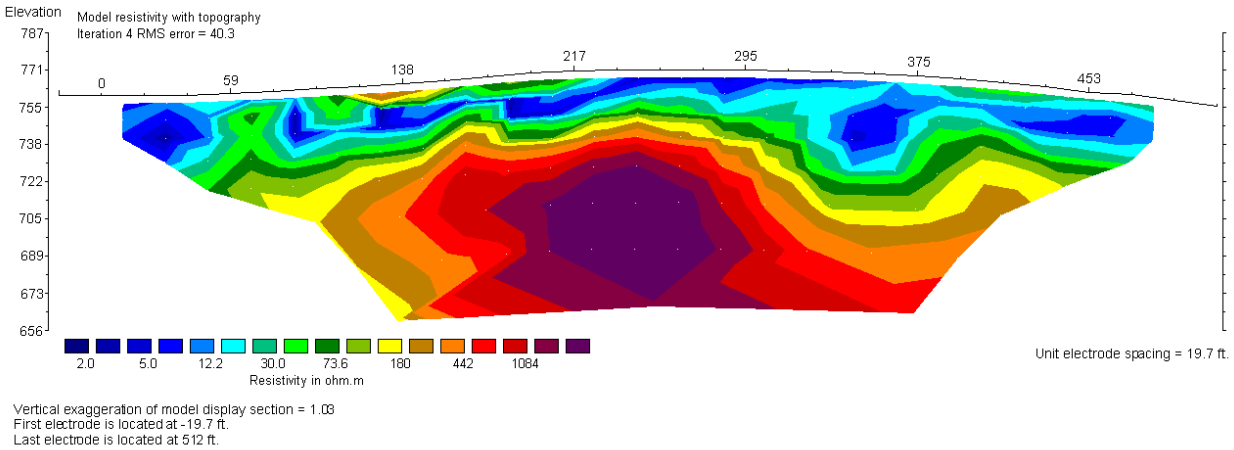


**Figure 27:** The same data as Figure 24 (dipole-dipole array), but with a different resistivity contour interval (note scale change). Also compare with Figure 26.

### 3.6.3 Results from Sting/Swift lines E and F

The results from lines E and F, which ran approximately N-S parallel to lines A, B and C, are shown in Figures 28 and 29. These lines cross the disturbed zone in a manner similar to lines B and C. RMS errors are larger in these figures than in the others, in part because the high-conductivity surface layer makes the potentials noisy. The RMS errors are reported as percent misfit, not absolute errors. This causes errors to appear large when the fit is actually quite satisfactory (i.e. a 1 ohm-m error is reported as a 20% error if the resistivity is 5 ohm-m). For Lines E and F, the fits are good, but appear to be significant because of the manner in which they are presented.

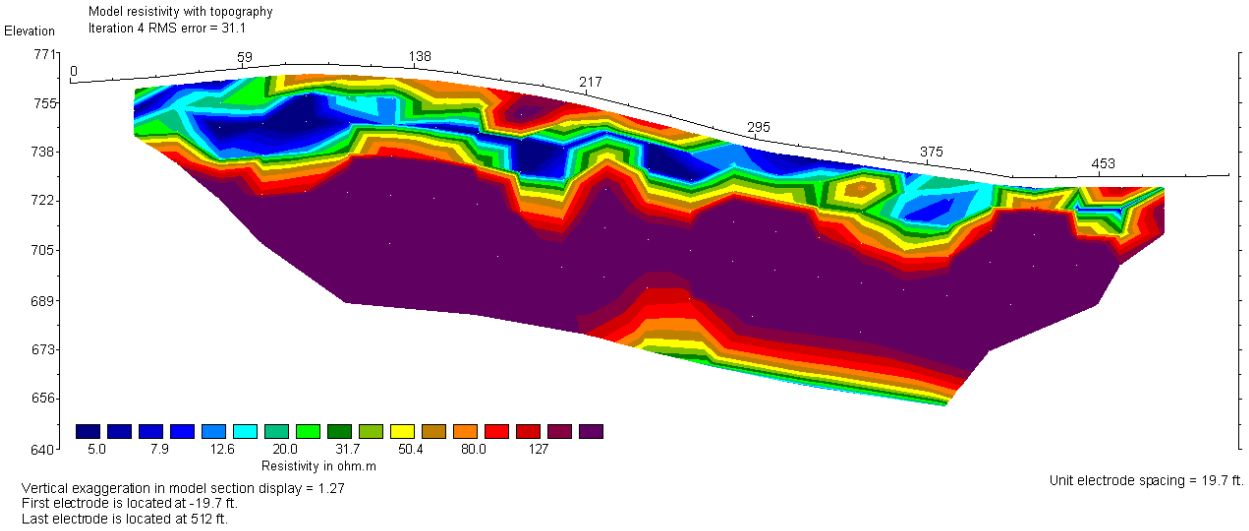


**Figure 28:** Line E runs parallel to lines A, B and C, and shows the same near-surface conductive layer. The burial ground begins at the southern end of this line.

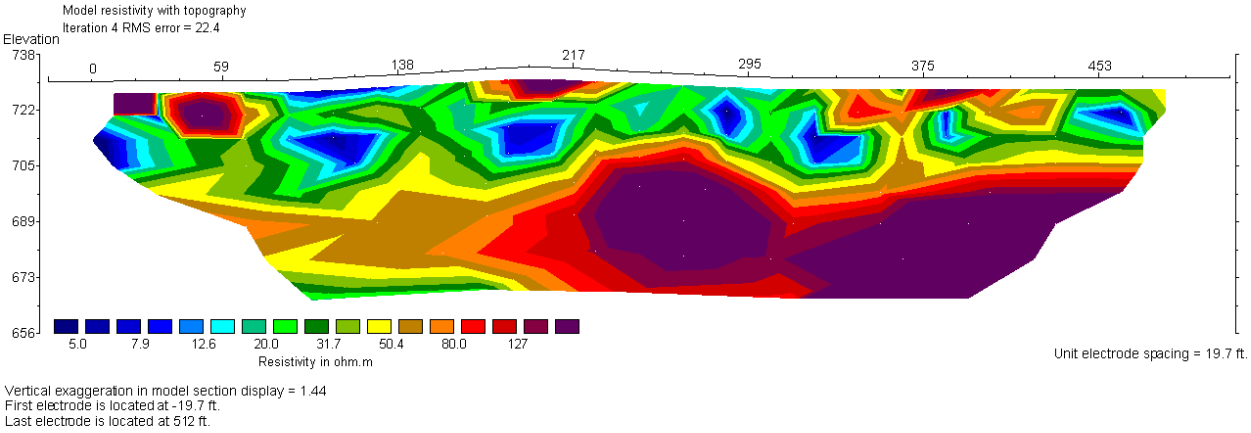


**Figure 29:** Line F shows the disrupted layering created by the burial ground for most of its length, but the southern end of this line appears to extend beyond the burial ground.

## 3.7 OhmMapper Surveys of the Landfill Area

The OhmMapper is a resistivity system marketed by Geometrics that is designed to collect resistivity data continuously along a profile. The transmitter and receiver are capacitively coupled to the ground, so there is no need to hammer electrodes into the ground. The system collects data in a dipole-dipole configuration, so by changing the separation between the transmitter and receiver the depth of investigation can be varied.

Doug Groom (Geometrics) demonstrated the OhmMapper at Camp Roberts by collecting data along the length of profiles B and C, and over all of block 15. The purpose of this demonstration was to show the OhmMapper's capabilities, and not to collect a complete data set over the landfill.

**Figure 30:** OhmMapper system: transmitter, receiver, tow cable, and control console. From Geometrics website.

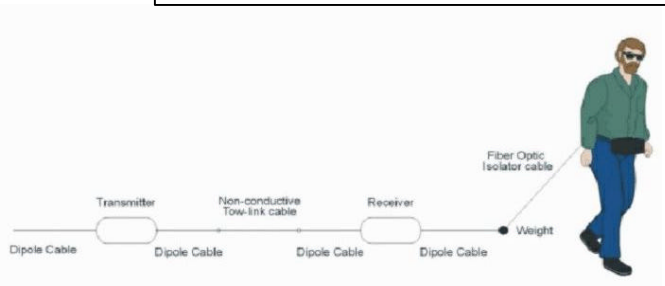


**Figure 31:** The operator tows the OhmMapper transmitter and receiver along the ground. The spacing between the dipole transmitter and receiver controls the sensing depth. From Geometrics website.

The OhmMapper collects makes tightly spaced measurements along the profile (roughly 1.5 ft spacing at a normal walking speed), but the profile must be repeated using different transmitter-receiver separations to build up a depth section (Figure 31). Geometrics collected data along the combined B-C profile using 10m transmitter and receiver dipoles, with separations between the transmitter and receiver of 16.4, 24.6, 32.8, 41.0, and 49.2 ft.

For the survey of Block 15, Geometrics collected data along 10 N-S lines spaced 32.8 ft apart. The transmitter and receiver dipoles were 32.8 ft, and all ten lines were repeated using separations between the transmitter and receiver of 16.4, 24.6, and 32.8 ft.

One of the principle advantages of the OhmMapper is that by capacitively coupling with the ground the system can collect resistivity data in areas where the near surface is extremely resistive, such as in northern Canada where the permafrost layer makes it virtually impossible to make good electrical contact with the ground using conventional resistivity systems. Conversely, in regions where the near surface is extremely conductive, as was the case at Camp Roberts, the capacitive coupling of the OhmMapper provides little signal penetration and the resulting data were noisy.

Inversion of the OhmMapper data for line B-C was accomplished using the same software (Res2Dinv) as for the Sting/Swift resistivity data (Figure 32). A stacked section that compares the Sting/Swift data (Figures 22 and 23) to the OhmMapper results (Figure 32) is shown in Figure 33.

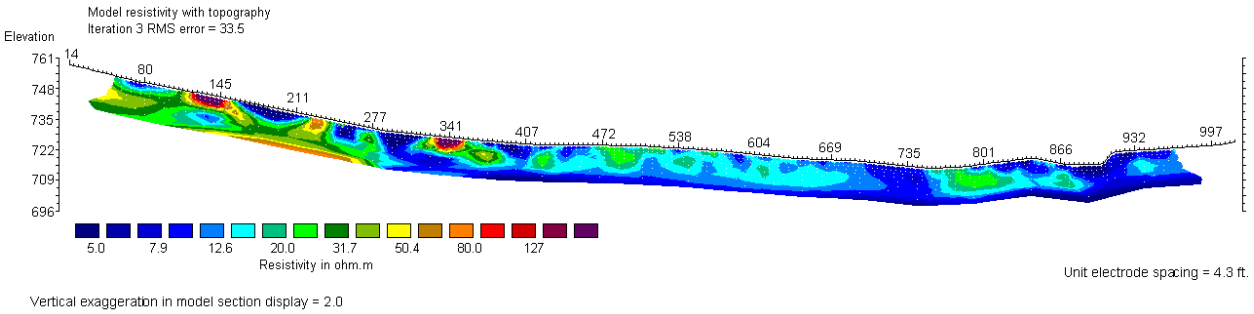


**Figure 32:** OhmMapper results for the B-C profile. North is to the left, south to the right.

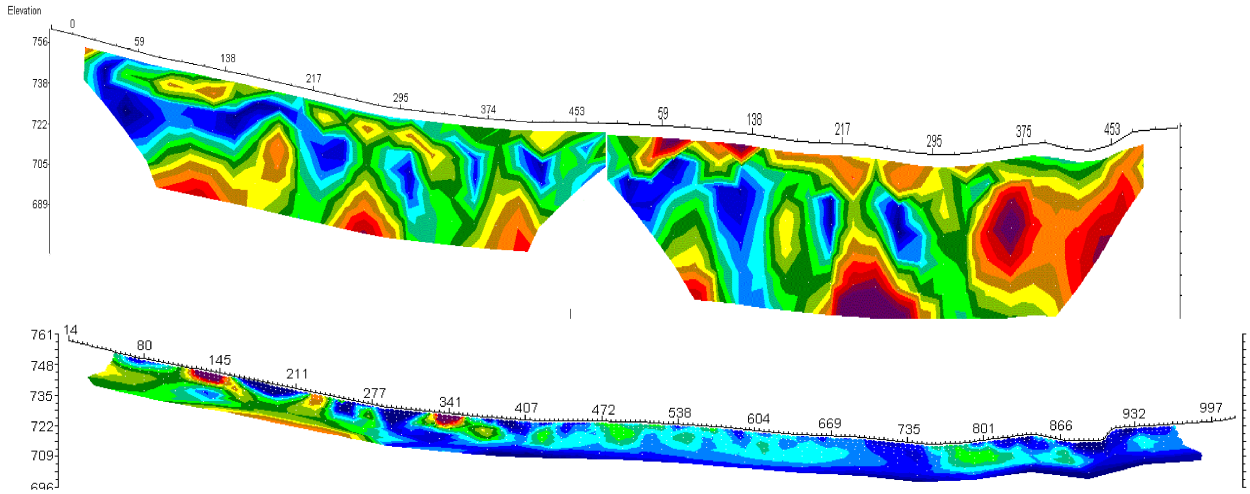


**Figure 33** Scaled stacked section, comparing the Sting/Swift results (top) with the OhmMapper results (bottom) for Lines B and C.

The OhmMapper results for Block 15 are provided in Figure 34. Only the results of profiling Block 15 with a 10 m dipole separation are shown here. The results for the 16.4 ft. and 24.6 ft. separations were very similar.

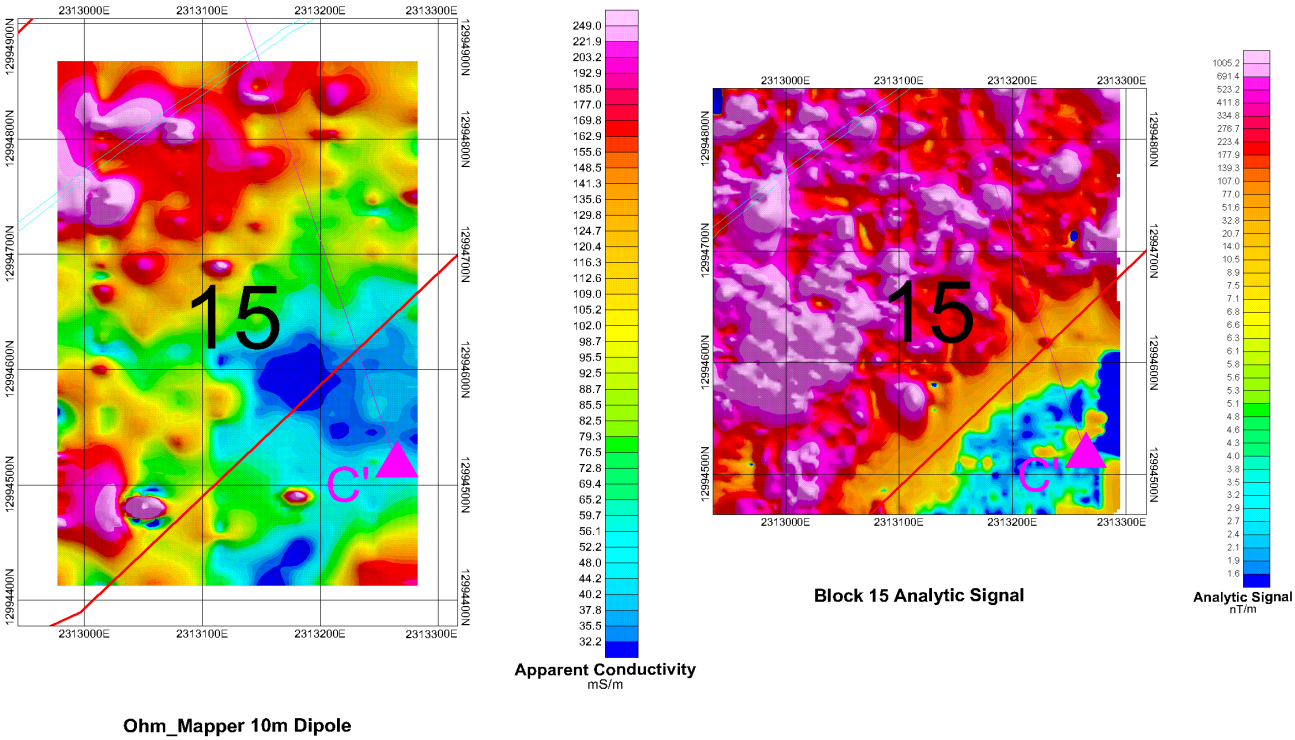


**Figure 34:** The OhmMapper data (left) and the magnetic analytic signal (right) show a similar pattern, although the magnetic data more clearly delineates the southern boundary of the burial ground (red line). The blue lines show the edges of the dirt road passing through Block 15, and the magenta line shows where profile line C crosses Block 15. Note that the OhmMapper data covers an area that is slight larger in the N-S direction and slight smaller in the E-W direction than the actual extent of Block 15 (shown in the magnetic data). Coordinates are UTM (ft).

# 4 Interpretation of Geophysical Data from the Landfill Area

## 4.1 Magnetic Data Interpretation

The analytic signal (total magnetic gradient) map of the landfill area (Figures 5 and 6) shows a very clear magnetic signature in the known landfill areas with only a few sporadic magnetic anomalies interspersed. The density of data points (at about 1-ft intervals along lines that are spaced 15-ft apart) makes it very unlikely that significant anomalies were missed. The high quality of the data is demonstrated by the absence of any striping parallel to lines of data points. Striping becomes apparent in magnetic data when there are significant deviations between adjacent lines, and these do not occur in the Roberts landfill data set. The correspondence between the mapped wells and boundaries of the landfill with the boundaries indicated by the magnetic data is excellent.

The anomalous region in the northwest portion of the map includes both the Permitted Landfill area and the South Unit (inactive) on Figure 1. Several wells within these mapped areas appear as large anomalies in the magnetic data (e.g. SVP-6, LS-3A, SVP-5, LS-4, and MW-4A) as does the 4-in steel standpipe at the easternmost corner of the South Unit. The fence between 2312600E 12995300N and 2312850E 12995550N, near the southern edge of the South Unit is also evident. The magnetic anomalies extend outside of the areas bounded by the South Unit and Permitted Landfill along the northeastern boundary of the South Unit (centered at 2312800, 12995600), and between the southeastern corner of the Permitted Landfill and well P-02.

The largest of the older mapped Waste Disposal Areas occurs dominantly in grid blocks 10, 14, and 15 of the magnetic data set (Figure 1), at the southeast corner of the map (Figure 3). This is shown on other references as the T1/T2 trench area (Geosystem Consultants Inc., 1998). As with the newer portion of the landfill that was described in the previous paragraph, the boundaries and wells correspond well between the magnetic data (Figure 3) and the site map (Figure 1). The northwestern boundary of the T1/T2 trench may extend slightly beyond the area that is mapped. However, some of the magnetic anomalies outside of the mapped boundary are almost certainly caused by metals that are within the boundary. Magnetic anomalies extend beyond the objects that cause them, particularly when those objects are at depth. The anomalous magnetic region similarly extends beyond the mapped area along the northeastern boundary of the T1/T2 trench, but the magnetic anomalies at the southeastern boundary are contained within the mapped portion of the landfill. A small anomalous area is associated with the road at the southern boundary of the map, presumably because of magnetic minerals in gravel or waste materials that were left along the side of the road.

Outside of the known waste sites, the most interesting anomaly is the EW trending feature between 2313000E 12995400N and 2313300E 12995400N. This corresponds roughly to an abandoned road or track used by our field crew to lay out resistivity lines Some of the anomalies are associated with intervening groundwater monitoring wells or standpipes (e.g. P-02, MW-6 and the standpipe at 2312650, 12994700, Figure 5). It is possible that other wells or standpipes, not included in the map database, could be responsible for other anomalies. Remaining anomalies are probably associated with metallic surface debris.

The homogenous background signature is an indication that native soils have a very low magnetic signature, as would be anticipated from silts, sands, and non-magnetic clays. Any magnetic minerals in the gravels are apparently sparse, or they occur at depths that would cause only small anomalies with our data acquisition parameters.

The traverses that extend south of the magnetic grid (Figure 7) show anomalies occurring as far south as 12993200. This extends a considerable distance beyond the southern limit of Trench T-3, but is consistent with the locations of other mapped trench areas (Trenches T-3, T-4, T-5, and T-6, Geosystem Consultants Inc., 1998). The disturbed zone can also be observed by surface inspection. Specific trench boundaries have not been compared for these southern traverses, as the data set is too sparse

## 4.2 Electromagnetic (EM-61) Data Interpretation

The mapped boundaries of the waste areas are confirmed by the EM-61 results from Area 14, which concur with the magnetic results from that section (Figure 8). The EM-61 results are easier to interpret because the EM data have a monopole response, unlike the magnetic data which produce a positive and negative component for each anomaly. The details of trench boundaries are easier to determine from the EM-61 data, which clearly shows three NE-SW trending anomalies, each presumably associated with a different trench.

The EM-61 data were more time-consuming to acquire because a GPS tracking system was not available for our use, and because it is slower and more awkward to tow the EM-61 cart than to use the shoulder-mounted magnetic sensors. In geologic settings where magnetic rocks are abundant, the EM-61 has a clear advantage. At Camp Roberts, both sensor systems are responsive to the landfills, and the magnetic system is an appropriate choice because of its ease of operation.

## 4.3 Seismic Data Interpretation

A four-layer model, derived with the time-intercept method, was used to represent each of the seismic lines at Camp Roberts. The velocities that were used were approximately 1180 ft/s, 2800 ft/s, 3800 ft/s, and 6300 ft/s. These velocities compare well with the velocities that were measured in the MW-1 vertical seismic profile (VSP). The velocity for layer 1, 1180 ft/s, could not be confirmed in the vertical seismic profile because this layer is so thin, but independent processing of the six profile lines yielded a consistent value for this layer. The velocities of the second and third layers are consistent between the wells and profile lines, but the depth of the boundary between layers 2 and 3 is markedly different between the profile data and downhole measurements at MW-1 (Figure 17). Re-examination of the data failed to provide a compatible solution. The incompatibility may be explained as the effect of a shallow high velocity layer that serves as a high velocity seismic refractor, but is underlain by a lower velocity zone. This could be caused by a perched water table, a shallow saturated zone associated with downward migrating moisture from earlier precipitation events, or a more highly compacted or cemented sediment zone (e.g. caliche), associated with the original depositional processes, cementation processes, or particle size. The gradational contact between layers 2, 3, and 4 lead to approximations in interface depths that are likely inaccurate.

The depth of the water table that was measured in MW-1 (602.8 ft elevation) is incompatible with the depth of the increase to velocities of about 6000 ft/s that occurs in both the VSP and the seismic refraction measurements. The measured water table occurs about 20 feet higher than the high velocity zone that is indicated at about 580 ft in the seismic data sets (Figure 17). Because this velocity transition occurs at similar depths in both the VSP and the seismic refraction results, it is unlikely that this velocity change is caused by the water table. The 20-ft. difference cannot be attributed to velocity inversions or heterogeneity of shallower sediments. It is likely that the velocity of layer 4 is either lithologic in origin, or that the "seismic water table", the velocity increases observed near the known water table, are associated with zones of partial saturation.

The seismic refraction model for Lines A, B, and C (Figure 13) shows a surface layer of variable thickness and low velocity, presumably associated with dry, unconsolidated sediments. The two underlying layers (2499 ft/s and 3842 ft/s) are not clearly differentiated in the data, and thus the contact between these two layers should be treated as a velocity contour in a gradational layer, rather than as an interface between two distinct units. The thickening and thinning of Layer 2 on Line C is coincident with the mapped boundary of the landfill (Figure 20), and is typical of the manner in which such features appear when layered models are used to represent seismic refraction measurements. The thickening and thinning of Layer 2 on Line C causes a sinusoidal disruption of the Layer 3/ Layer 4 contact beneath Line C, and an abrupt depth change for that interface where Line B and Line C meet (470 feet distance, 500 ft elevation on Figure 13). The tops of Layers 3 and 4 are much more continuous laterally on Lines A and B, indicating that the near surface is less disturbed. Layer 4 varies between about 570 and 610 ft elevation while Layer 4 is flatter with an elevation of about 730 ft at the north end and about 710 ft at the south end.

The RAYFRACT tomographic image for Lines B and C (Figure 18) appears to provide a more reliable representation of the subsurface. The velocity gradient (continuous increase in velocity with depth rather than abrupt layer changes) is apparent in this image, but the gradient is not constant over the length of the section, indicating significant lateral heterogeneity. High velocity zones at 500 and 725 ft (distance) and about 50 ft beneath the surface correspond well with the northern and southern boundaries of the waste areas (Figure 20). The depths of the zones are probably too large, and may indicate a limitation of the inversion for data acquired with these parameters. A steep velocity gradient occurs along an irregular surface at about 500 ft depth, particularly on the southern half (Line C) of the section. The structure on this surface may be an artifact caused by the disturbed near surface zone, or it could represent an irregular bedrock surface that underlies the site. Portions of the image that are below about 500 ft elevation should be treated with caution, as they are not well constrained by the data, particularly near the northern and southern margins of the image. It is noteworthy that no clear boundary corresponds with the mapped water table depth, as was noted earlier for the time-intercept section for these lines.

The tomographic result for Lines B and C clearly demonstrates that a tomographic solution is much more appropriate to the Camp Roberts data than the time-intercept solution. Not only does it provide a credible representation of the trench area, but it also shows the velocity gradient and absence of layering that were problematic in the time-intercept results. The interpretations of time-intercept results for Lines A, D, E, and G should be treated with caution with the tomographic results in mind.

The conventional (SIP delay-time) model for Line D showed a poor fit for layer 3, and the first arrivals could not be identified that correspond to layer 4. Therefore, the model shown in Figure 14 includes only the Layer 1 / Layer 2 interface. The velocity for Layer 2 is higher than for the other five sections. We interpret this to be an indication of a high degree of heterogeneity on Line D. We note that this line is orthogonal to the predominant orientation of the others, and this may indicate that the heterogeneity is more severe in the east-west direction than in the north-south direction.

We were unable to detect Layer 4 on Line E data, but the other interfaces in the delay-time model (Figure 15) are well constrained and similar in character to those in Lines A,B, and C. The thickening of Layer 1 and variability of the Layer 2 / Layer 3 interface at the south end of the line may be due to a disturbed near surface associated with the mapped trench location. If so, it is interesting to note that the effect is not as pronounced as it is along Line C, perhaps because Line E does not cross the disposal area as much as Line C.

The time-intercept model for Line G (Figure 16) shows layers that are smoothly varying with none of the radical variations that were observed on Line C. Layers 2 and 3 show a thinning at about 370-380 ft, and Layer 4 shows a small but abrupt transition at that depth. The location of these features corresponds with the location of the monitoring well, MW-1, and may be related to compaction or minor disruption of the surface that occurred during drilling. The elevation of the top of Layer 4 is in the same range as it was beneath Lines A, B, and C, at 570-610 ft.

Bedrock depth at the landfill site has not been determined by drilling. Two possibilities may be considered from the seismic refraction results. First, it is possible that Layer 4, which ours at elevations of 570-610 ft, could represent a low-velocity bedrock interface. The well logs indicate that a transition from conglomeratic sandstone to conglomerate occurs at 118 ft depth (575 ft elevation), but there is no indication of any significant accompanying change in cementation, weathering, or induration. The absence of a steep velocity gradient in the 570-610 ft elevation range in the tomographic inversion for Lines B and C provides additional indication the velocity increase at 570-610 ft elevation is not associated with bedrock.

A second possibility is that the high-velocity zone (9000-10000 ft/s) at about 450-550 ft in the tomographic inversion for Lines B and C (Figure 18) could represent the bedrock interface. The velocity is more typical of bedrock, and the steep gradient is a better representation of the contrast that would be expected at a bedrock/sediment interface.

## 4.4 Multielectrode Resistivity Data Interpretation

Several points should be kept in mind when interpreting the resistivity cross sections: First, the inversion process that translates raw resistivity data into a resistivity cross section is non-unique. More than one possible subsurface configuration could result in the measured data. The inversion program chooses the smoothest, least heterogeneous, solution. This solves the mathematical problem of non-uniqueness, but produces a slightly blurred image of the actual geology. Abrupt transitions between layers become gradational transitions in the resistivity section.

Second, the data are collected along a line and inverted assuming two-dimensional geologic structure. This assumption is reasonable for a layered earth, or for dipping layers if the data are collected perpendicular to strike, but works less well over localized three-dimensional targets such as buried metal objects. The resistivity data will still show the target, but the dimensions will not be correct.

Finally, it is important to realize that this geophysical technique maps changes in resistivity, which may or may not correspond to changes in geologic formation. Resistivity changes can occur within a formation, and conversely, two formations may have the same resistivity and be indistinguishable on the resistivity section.

Starting at the top of the hill with Line A (Figure 21), we notice first that the entire section has very low resistivity values – all less than 200 ohm-m. We believe that this is because of the high clay content of the soil, and the presence of evaporites (salts). The drilling logs for the area wells refer to the local Paso Robles Formation as, "SILTY CLAY, dark to moderate yellowish brown, stiff non-plastic, dry to moist, with fine- to medium-grained sand, friable, caliche or gypsum along fracture openings." Clay has a low electrical resistivity, and if the pore water is saline, the resistivity will be lower still.

Evaporites may explain the layering visible in line A. It rained in the weeks preceding our survey, but was dry during our fieldwork. The surface probably dried out, creating a thin resistive zone. Beneath this there is a very low resistivity layer (<10 ohm-m) that probably corresponds to moist, salty clay. The resistivity increases again below about 33 ft. This could be either a moisture change or a lithology change. Note that the magnetic data give no indication of metal buried under this line, so the resistivity variations probably correspond to soil and rock changes, not buried waste.

Line B (Figure 22) enters into the southern disposal area (inactive) at the south end (see Figure 20). The resistivity data show the same general pattern as we saw for line A, but the layering appears to be disrupted at the south end, probably because of the landfill excavation and fill. It is not clear that the metal within the landfill can be distinguished in the resistivity data because the host material already has a very low resistivity. The differences between an extremely good conductor (salty clay) and a near-perfect one (metal) are very subtle.

It is unclear whether the resistivity data can be used to determine the depth of the fill. The disruption of the layering appears to extend to the full depth of the cross section (roughly 50 ft); it seems unlikely that material was buried this deep.

Line C, which lies almost entirely within the southern disposal area, shows the same disrupted layering (Figure 23). Interestingly, the very southern end of line C extends beyond the south end of the burial ground according to the magnetic data, yet the near surface conductive layer is still missing in the resistivity data. In fact, that portion of the line is relatively resistive. The questions is whether the magnetic data shows the true southern boundary of the burial ground and there is simply no conductive soil layer present, or the whether burial ground extends further but has no ferrous metal buried further south, and consequently no magnetic anomaly.

The resulting resistivity cross section for Line D (Figure 24) shows the same near-surface conductive layer as in line A, over a slightly more resistive material beginning at a depth of about 10-20 ft. Notice that the conductive near-surface layer is unbroken, which is consistent with the line being outside of both burial grounds.

The data from all of these lines are quite noisy because this conductive near-surface layer acted as a virtual short circuit, and made it difficult to drive current deep into the ground to probe deeper structure. This problem was accentuated by the use of a dipole-dipole array.

It is interesting to compare the results for Line D from the test run using the dipole-dipole array (Figure 24) with the results for the same line using a Schlumberger array (Figure 26). The basic patterns are the same: both show an extremely low resistivity layer near the surface, and a more resistive layer below. The two differ in detail, however, and this illustrates the why it is important not to read too much into the fine detail of the resisitivity contours. The results of the Sclumberger array show a smoother near-surface layer (less noise, but less detail).

At depth, the uniformity of the results of the dipole-dipole array is an artifact of the choice of resistivity contour intervals. The dipole-dipole data with a different scale shows variation at depth. With the exception of Figure 27, we have used the same resistivity scale for all of the Sting/Swift results. This makes it easier to compare lines, but does not bring out all of the detail in each line. Our data analysis involved plotting all of the resistivity lines using a variety of scales, comparing dipole-dipole and Schlumberger array results, and the results of inverting the data with different parameter settings. Due to space constraints, only a portion of these figures is present in this report.

The inversion results for Lines E and F (Figures 28 and 29) show similar structure to that in Lines A, B, and C. Line E shows the near-surface conductive layer which is disrupted near the base of the hill, where line F starts, over the burial ground. This disruption is evident for nearly all of line F, which extends beyond the magnetic grid. The very southern end of line F shows what appears to be a return to the natural layering, suggesting that the line extends beyond the southern boundary of the old burial ground, in agreement with site drawings.

Preliminary processing of the resistivity data shows good agreement with the magnetic data. The burial ground shows up as a disruption of the lithologic layering. However, the low-resistivity soils in this area make it difficult to detect buried metal targets.

## 4.5 OhmMapper Data Interpretation

The results show about 13 ft of penetration (Figure 32), and the same highly conductive near-surface layer as in the Sting/Swift data. Interestingly, the OhmMapper appears to show the transition to the burial ground, which occurs near the base of the hill at about 278.9 ft in Figure 32, as a change to an even higher conductivity. This was not the case with the Sting/Swift, suggesting that the OhmMapper is more sensitive to buried metal than DC resistivity, or that the because the OhmMapper was sensitive to only upper first four meters of the subsurface, buried metal had a proportionally larger effect on the resistivity data.

The OhmMapper results for Block 15 also demonstrates the sensitivity of the OhmMapper to the buried metal within the boundary of the old landfill (Figure 33). The southwest corner of Block 15 extends beyond the southern boundary of the landfill, and the OhmMapper data show a corresponding decrease in conductivity in the southeast corner.

The OhmMapper data in Figure 33 have been plotted as conductivity values, the reciprocal of resistivity, to make it easier to compare the results with the magnetic analytic signal results for Block 15. We expected conductivity to increase where magnetic field strength increased, and this is shown to be the case when we compare the OhmMapper results to the magnetic analytic signal in Figure 33. Note that this is only a qualitative comparison because the two instruments, the OhmMapper and the magnetometer, are responding to two different physical properties, electrical conductivity and magnetic susceptibility respectively. Although we expect both to be greater over buried metal, the presence of evaporates in the soil has a large influence on the conductivity, but none on the magnetic response.

Although the conductive soils present in the landfill area limited the penetration of the OhmMapper and increased the noise levels, the OhmMapper still provided interesting results. The horizontal resolution was superior to the Sting/Swift multielectrode resistivity system because of the tightly spaced samples (1.6 ft vs. 19.6 ft for the Sting), but penetration was worse (13 ft vs. 80 ft for the Sting).

The OhmMapper proved far superior to the Sting/Swift as a rapid profiling tool. Collecting ten OhmMapper lines at three dipole spacings over Block 15 took only a few hours. To collect the same ten lines with the Sting would have taken about ten times as long. Although the magnetic data were superior for delineating the boundary of the landfill, the OhmMapper performed adequately, and would work well for burial grounds containing only non-magnetic targets such as asbestos, or fiberglass tanks, where the magnetometer would not. The demonstration, although covering only a limited area, successfully highlights the strengths and weaknesses of the OhmMapper system, keeping in mind that the system would have performed even better in a more electrically resistive environment.

## 4.6 Summary Interpretation

*Landfill boundaries*
The magnetic results clearly define the boundaries of the active and historic landfills, and show no evidence of trenches or buried wastes between them. The EM-61data provide a similar result, though the data are more time-consuming to acquire. GPS positioning systems are available for use with the EM-61, and would shorten the time required for acquisition. The landfill boundaries that are defined in map view by the magnetic data and the EM-61 data are supported in profile by the seismic refraction data and multielectrode resistivity data. The seismic data are most effective in identifying trench locations when a tomographic inversion is used, instead of a conventional delay-time approach to interpretation. This shows a localized high-velocity zone that coincides with the trench boundaries that are defined by the magnetic data. The multielectrode resistivity data show a disruption of layering where trenching has occurred.

*Water table*
None of the data sets were able to reliably detect the water table. High conductivity layers in the near-surface limited the penetration of the resistivity system. Correlation of seismic refraction results and the VSP at MW-1 with the measured water table showed a 20-ft offset between a zone of seismic velocity increase and the measured water table elevation that we were unable to explain.

*Bedrock depth*
As indicated earlier, no method that we tested showed a clear response to bedrock. Without ground truth data from wells, we are presently unable to address this issue. Tomographic processing of the remaining seismic refraction lines might provide a clearer indication of the depth and character of the bedrock interface, particularly if these data are tied to well measurements. The absence of an abrupt velocity increase that is typically associated with bedrock suggests bedrock is very deep, or that the bedrock has the same composition as overlying sediments that are less compacted and/or uncemented, and that the lithification processes are gradational over a large depth range.

*Heterogeneity*

Both the seismic data and the multielectrode resistivity data provide evidence that the shallow geology is laterally discontinuous and heterogeneous. This could include zones of caliche, perched water, and/or facies changes associated with fluvial deposition that would include (at a minimum) sandstones, mudstones, and conglomerates. Such a geologic setting demonstrates the limitations of geophysical analysis methods that assume lateral continuity and which disallow gradational changes in physical properties. In the case of the seismic data, the geologic setting is much better suited for processing with a tomographic inversion approach than a conventional delay-time method. The high electrical conductivity of the near surface imposed limitations on the penetration depth of both the OhmMapper and multielectrode resistivity systems. The multielectrode system was better suited for penetrating this zone than was the OhmMapper.

# 5 EM-61 Survey of the Tank Site

## 5.1 Introduction

The goal of the electromagnetic data collection at this site was to locate buried drums or underground storage tanks (UST) that were suspected near a refueling station.

A standard Geonics EM-61 metal detection instrument was used. The grid was established in an arbitrary projection so that the survey lines were oriented parallel to the refueling station. The grid point 225E 125N is located at the SW corner of the concrete pad supporting the refueling tanks. The 225E meridian lies along the long axis of the pad from the SW to NW corners.

Data were recorded on a constant time interval of 10Hz. The instrument was calibrated for background readings at a relatively non-conductive area to the SW of the grid. Navigation and positioning were based on taped lines 4 feet apart with markers every 25 feet. Data from the upper coil and lower coil are presented, along with the difference between the two. No filtering was required.

In addition to the NS grid lines, three lines were run EW over the strongest anomaly response. After surveying, the instrument calibration was re-checked at the original calibration point to verify the absence of electronic drift.

## 5.2 Interpretation of the Tank Site data

The three parameters shown here emphasize three different aspects of the area. The color distributions have been adjusted to enhance these features. The lower or bottom coil is best suited for detection of larger objects. In Figure 35, four anomalies are clearly seen. Anomaly B is a suspected UST or trench of drums. Anomaly C is associated with the concrete pad of the refueling station. Anomalies A and D are unknown.

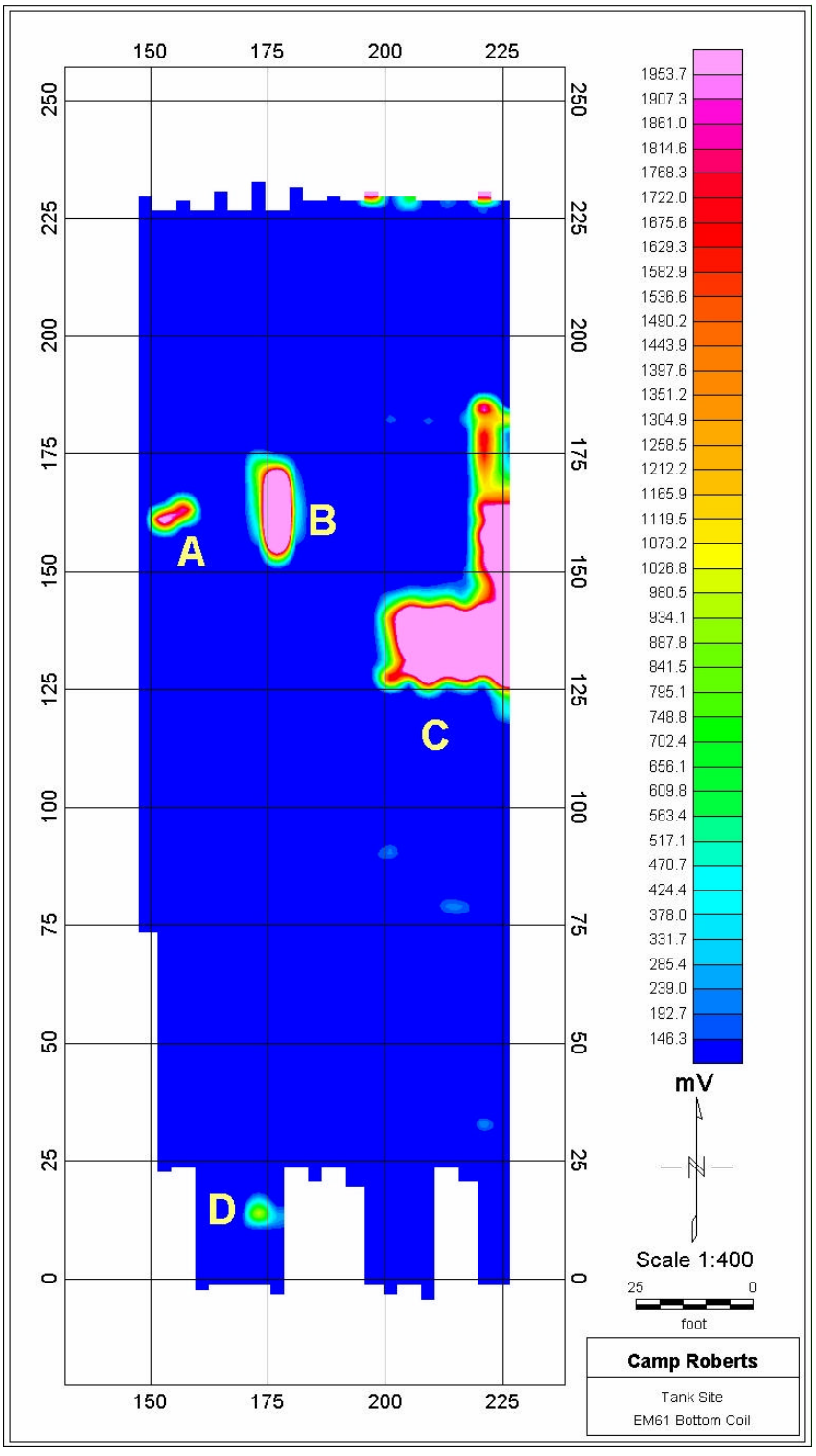


**Figure 35:** EM61 bottom coil with course color scale to illustrate major features.

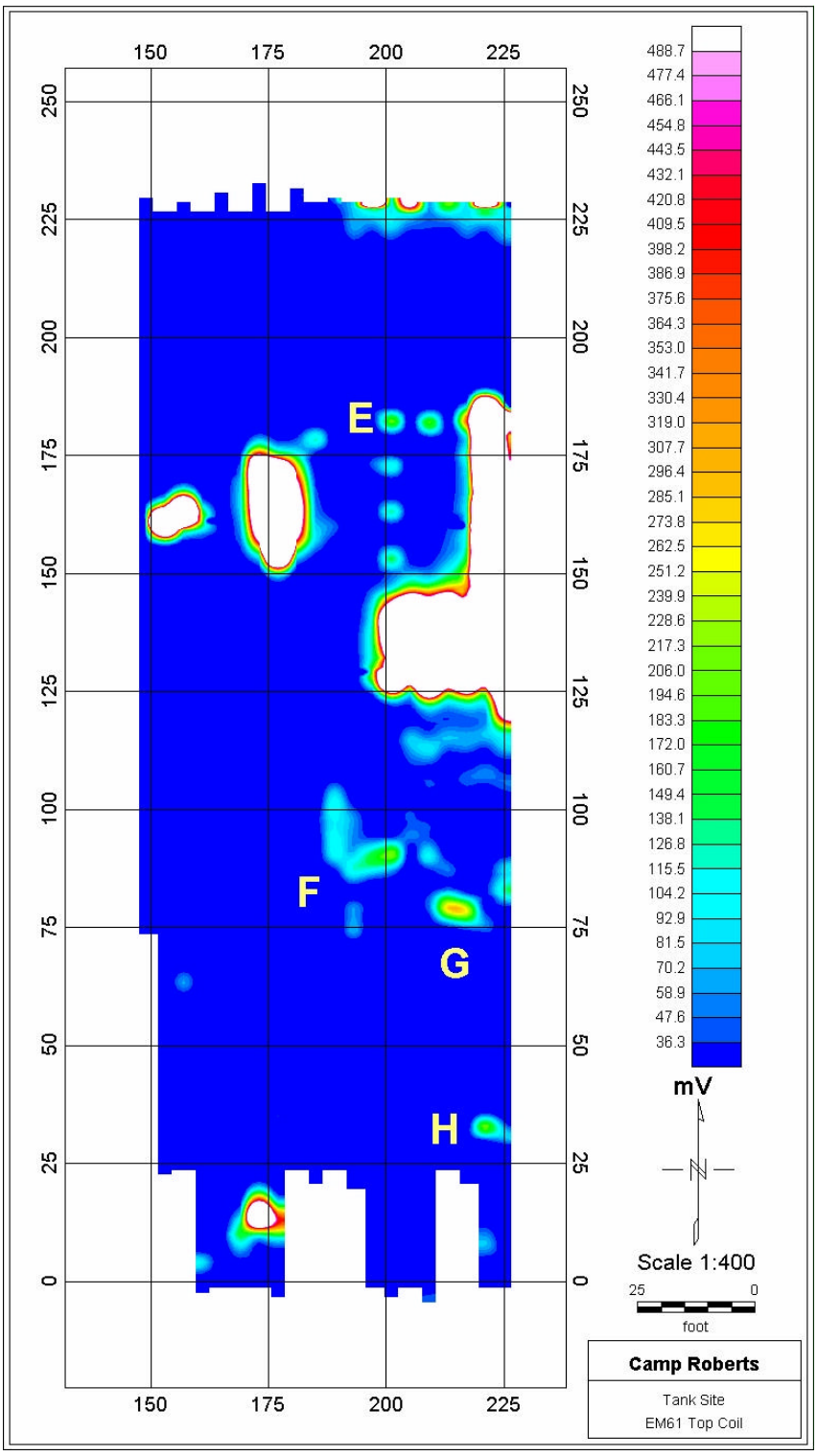


**Figure 36:** EM61 top coil data with medium color scale to illustrate moderate sized targets.

In Figure 36, the upper coil is shown to illustrate smaller targets of possible significance. The anomalies at location E may represent individual drums or pipes. The anomalies at F, G and H are unknown, but may also be related to multiple buried drums.

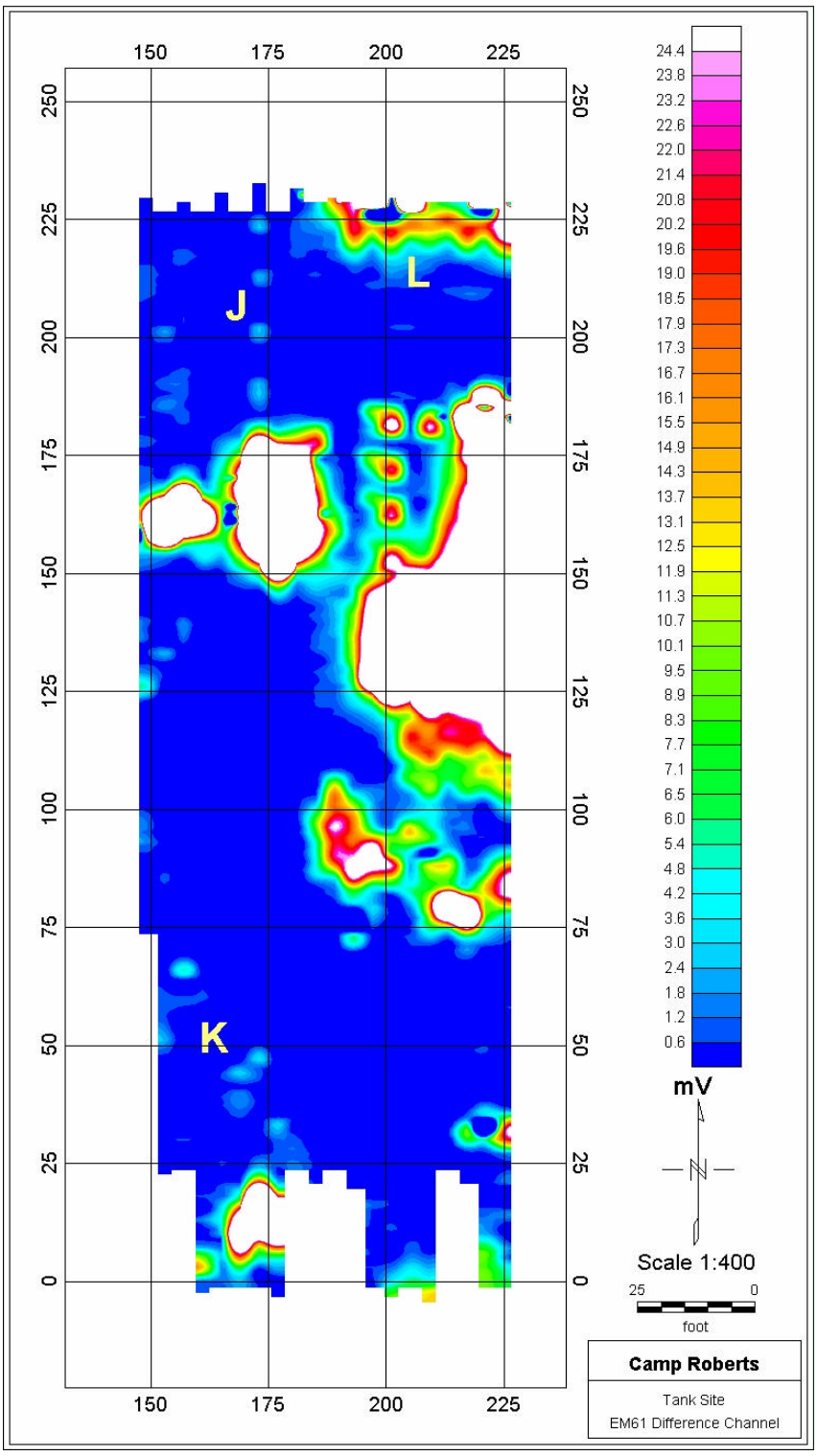


**Figure 37:** EM61 difference data (bottom coil minus top coil) with fine color scale to highlight the most subtle features.

In Figure 37, the difference between the upper and lower coils is presented to illustrate the finest level of detection capabilities. The anomalies at J may represent individual drums at extreme depth (4-5m). The anomalies at K are more likely small surficial items. The anomalies at L reflect the presence of another concrete pad off the end of the survey block.

# 6 Recommendations

The data acquired in this project can be used to guide future applications of geophysical techniques at Camp Roberts. For instance, if further definition of the southern portion of the historic landfill is needed, the magnetic mapping method that was used in this study could be adapted to cover that area. Depending on the precision that would be needed, a coarser line spacing might be used than was used in this study. The results also demonstrate that the site is well suited to magnetic acquisition methods. If a large area (e.g. > 200 acres) must be surveyed (e.g. a survey of a target range for UXO), a helicopter-based airborne magnetic method would be very effective at this site, and might be expected to detect objects containing as little as 2 kg. of ferrous iron. The EM-61 was similarly proven to be an effective tool at Camp Roberts for detection of buried metallic waste.

If it is important to map the bedrock surface, geophysical methods could be used in conjunction with confirmatory drilling to map the interface. One possible interpretation of the tomographic refraction image (Figure 18) is that the bedrock interface is very irregular. If such is the case, a program that relied on drilling would be ineffective. Electromagnetic methods that have better penetration than those used in this study (e.g. Controlled Source Audio Magnetotellurics – CSAMT, or Time-domain Electromagnetic Methods, TDEM) could be used in conjunction with tomographic seismic refraction methods to produce a reliable bedrock map. The electromagnetic methods that are mentioned above might also provide a better estimate of the water table depth

# 7 Acknowledgements

Barry Kinsall, Don Rock, Jon Cunningham, John Zutman and Frank Gardner provided superb field support for this project. Doug Groom (Geometrics) acquired the OhmMapper data and provided it at no cost. Siegfried Rohdewahl, Intelligent Resources Inc, inverted the seismic data from Lines B and C at no cost to the project. Guy Romine (Los Alamitos Office of the Naitonal Guard Bureau) provided an interface with the Camp Roberts staff as well as extensive field support. Rob Huggins (Geometrics) provided surface and downhole seismic cables at no cost to the project. Philip Miller (Geosystem Consultants, Inc.) and Bob Pettit (Aero Geodetic Corporation)were very helpful in providing site maps and data bases from work at the site. Finally, we would like to thank Wayne Mandell (AEC) for providing the inspiration and support for this project.

# 8 References

EMCON Associates, 1990, Water Solid Waste Assessment Test Interim Report, Camp Roberts Sanitary Landfill, San Luis Obispo County, California, 23 pp., June 1990.

Environmental Science Associates, Inc, 1989, Geoloic map of Camp Roberts, California, Scale: 1:25,000, derived from Camp Roberts Environmental Management Analysis Plan, February 1989.

Geosystem Consultants, Inc., 1998, Groundwater and vadoze zone monitoring, third quarter 1998, Solid waste disposal facilities, Camp Roberts, California, provided as a PDF file on CD-ROM.

Rimrock Geophysics, 1995, User's guide to SIPx programs,1995.

Smith, Gardner, and Dunne, Inc., 1989, Water Quality Solid Waste Assessment Test, Camp Roberts Sanitary Landfill, San Luis Obispo County, California, June, 1989.